

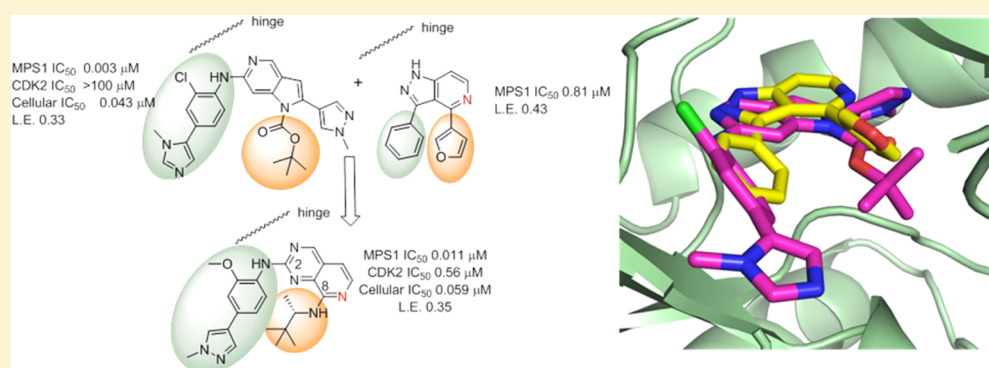
Rapid Discovery of Pyrido[3,4-*d*]pyrimidine Inhibitors of Monopolar Spindle Kinase 1 (MPS1) Using a Structure-Based Hybridization Approach

Paolo Innocenti,[†] Hannah L. Woodward,[†] Savade Solanki,[†] Sébastien Naud,[†] Isaac M. Westwood,^{†,‡} Nora Cronin,[‡] Angela Hayes,[†] Jennie Roberts,[†] Alan T. Henley,[†] Ross Baker,[†] Amir Faisal,^{†,||} Grace Wing-Yan Mak,[†] Gary Box,[†] Melanie Valenti,[†] Alexis De Haven Brandon,[†] Lisa O'Fee,[†] Harry Saville,[†] Jessica Schmitt,[†] Berry Matijssen,[†] Rosemary Burke,[†] Rob L. M. van Montfort,^{†,‡} Florence I. Raynaud,[†] Suzanne A. Eccles,[†] Spiros Linardopoulos,^{†,§} Julian Blagg,[†] and Swen Hoelder^{*,†}

[†]Cancer Research UK Cancer Therapeutics Unit, Division of Cancer Therapeutics, The Institute of Cancer Research, 15 Cotswold Road, Sutton, London, SM2 5NG, United Kingdom

[‡]Division of Structural Biology and [§]Breast Cancer Now, Division of Breast Cancer Research, The Institute of Cancer Research, 237 Fulham Road, London, SW3 6JB, United Kingdom

S Supporting Information



ABSTRACT: Monopolar spindle 1 (MPS1) plays a central role in the transition of cells from metaphase to anaphase and is one of the main components of the spindle assembly checkpoint. Chromosomally unstable cancer cells rely heavily on MPS1 to cope with the stress arising from abnormal numbers of chromosomes and centrosomes and are thus more sensitive to MPS1 inhibition than normal cells. We report the discovery and optimization of a series of new pyrido[3,4-*d*]pyrimidine based inhibitors via a structure-based hybridization approach from our previously reported inhibitor CCT251455 and a modestly potent screening hit. Compounds in this novel series display excellent potency and selectivity for MPS1, which translates into biomarker modulation in an in vivo human tumor xenograft model.

INTRODUCTION

Interfering with mitotic processes has been a successful therapeutic approach to fight cancer.¹ One example of a mitotic target is monopolar spindle 1 (MPS1, also known as TTK), a dual-specificity kinase that occupies a central role in the transition from metaphase to anaphase and is one of the main components of the spindle assembly checkpoint (SAC).² This kinase prevents cells from progressing through mitosis until the kinetochores are properly attached to the microtubules and are under the appropriate tension. While this mechanism is important to ensure error-free segregation of chromosomes in normal tissues, aneuploid and chromosomally unstable cancer cells often overexpress, and are particularly dependent on, MPS1 to cope with the stress arising from abnormal numbers of chromosomes and centrosomes.³ Due to these findings, it is not

surprising that MPS1 is upregulated in a number of tumor types⁴ and that higher levels correlate with higher histological grade, aggressiveness, and poorer patient survival in breast cancer, glioblastoma, and pancreatic ductal adenocarcinoma.^{4a,5} Furthermore, phosphatase and tensin homologue (PTEN)-deficient breast cancer cell lines have been reported to be more sensitive to MPS1 depletion or kinase inhibition.^{3b,6}

Using advanced inhibitors, including our own 1 (CCT251455, vide infra),⁷ effective dosing schedules have been investigated in vivo. Importantly, it has recently been shown that MPS1 inhibitors have a relatively narrow therapeutic window^{5a,8} and that they are particularly effective when used in combination

Received: November 20, 2015

Published: April 7, 2016

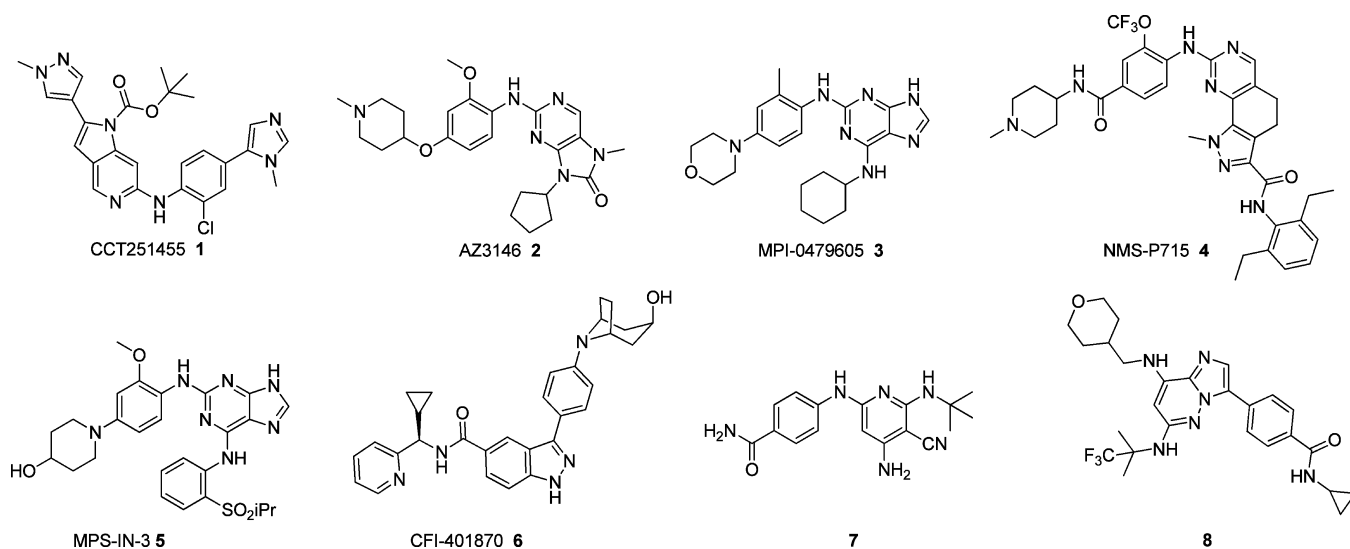
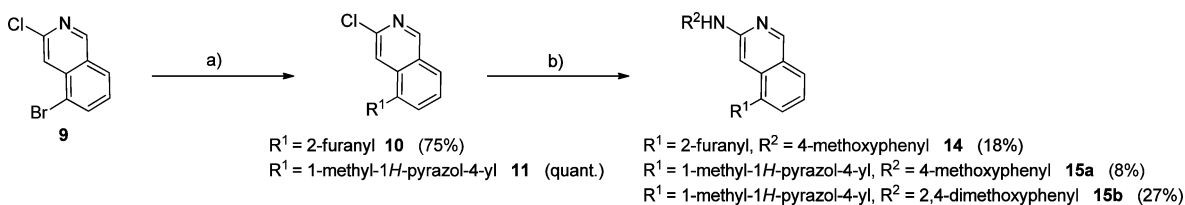


Figure 1. Published MPS1 inhibitors.

Scheme 1. Synthesis of Isoquinoline Derivatives^a



^aReagents and conditions: (a) Furan-2-ylboronic acid or 1-methyl-4-(4,4,5,5-tetramethyl-1,3,2-dioxaborolan-2-yl)-1H-pyrazole, Na_2CO_3 , $\text{Pd}(\text{dppf})\text{Cl}_2 \cdot \text{CH}_2\text{Cl}_2$, DME/water, μW , 105 °C; (b) 4-methoxyaniline **12** or 2,4-dimethoxyaniline **13**, $t\text{BuXPhos}$, Pd_2dba_3 , Cs_2CO_3 , $t\text{BuOH}$ /water, μW , 80–100 °C. Reaction yields are in parentheses.

with, for example, tubulin-targeting agents such as paclitaxel or CDK4/6 inhibitors.⁹

Several MPS1 inhibitors have been disclosed,¹⁰ these include AstraZeneca's AZ3146 (**2**),^{10b} the Myrex compound MPI-0479605 (**3**),^{8c} and the Nerviano compound NMS-P715 (**4**).¹¹ Also described in the literature are MPS-IN-3 (**5**),^{5a} CFI-401870 (**6**),¹² and the Shionogi compounds (**7**, **8**) (Figure 1).^{8a,13}

We recently disclosed a series of 1H-pyrrolo[3,2-c]pyridines exemplified by the potent and selective chemical probe **1**.⁷ However, while this compound showed excellent potency in biochemical and cellular assays, other properties hampered further development. In particular, **1** has a relatively high molecular weight (504) and AlogP (5.7) and also featured a *tert*-butoxycarbonyl (Boc) moiety that appeared critical for potent inhibition but unsurprisingly proved to be unstable under strongly acidic conditions.¹⁴ In addition, **1** was a potent cytochrome P450 (CYP) inhibitor ($\text{IC}_{50} < 1 \mu\text{M}$ observed for CYP 1A2, 3A4, 2C9, 2C19, 2D6) which represented a significant issue not least because MPS1 inhibitors are reported to be particularly effective in combination with other chemotherapeutic agents, e.g., paclitaxel. To mitigate the risk that these undesirable features were inherent to the 1H-pyrrolo[3,2-c]pyridine series, we set out to discover a second structurally unrelated chemotype featuring a clean CYP profile, no acid labile groups, and significantly lower molecular weight and lipophilicity. We thus set out to discover an additional lead series that (a) showed potent inhibition of MPS1 in cellular assays ($\text{IC}_{50} < 100 \text{ nM}$), (b) showed good ligand efficiency (L.E. ~ 0.35),¹⁵ (c) displayed excellent selectivity, in particular against

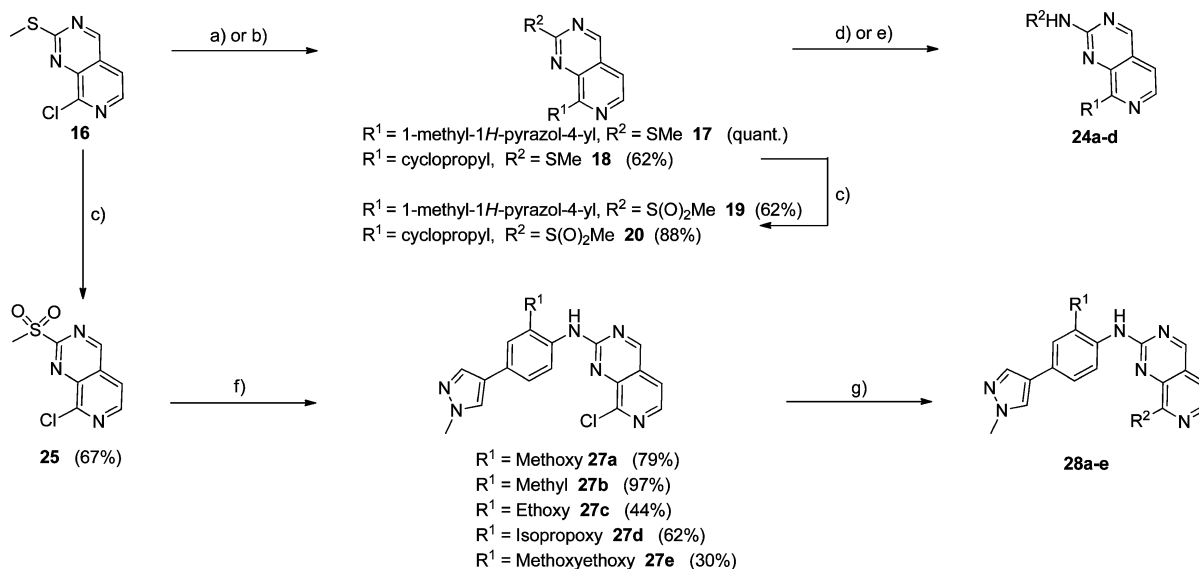
other cell cycle kinases such as cyclin-dependent kinase 2 (CDK2), Aurora A and B, and more generally against the wider kinome (K_i ratio >100), (d) robustly modulated MPS1 kinase activity in a human tumor xenograft PK/PD model, and (e) showed significant scope for further modification.

Herein we describe the rapid discovery of such a series by structure-based hybridization of the 1H-pyrrolo[3,2-c]pyridine series and a modestly potent hit from a focused kinase library screen. This completely new MPS1 series featured an unexploited kinase chemotype (the pyrido[3,4-d]pyrimidines) and advanced examples displayed subnanomolar K_i s and excellent overall selectivity. The favorable *in vitro* properties translated into biomarker modulation in an *in vivo* human tumor xenograft model.

CHEMISTRY

The synthesis of isoquinolines **14**, **15a** and **15b** was carried out from the commercially available 5-bromo-3-chloroisoquinoline **9** through sequential Suzuki couplings and Buchwald reactions using suitable boronic acids or esters and the required anilines (Scheme 1).

Compounds **24a–d** and **28a–e** in the pyrido[3,4-d]pyrimidine series were prepared according to a previously described strategy which makes use of the novel 8-chloro-2-(methylthio)pyrido[3,4-d]pyrimidine building block **16**.¹⁶ Thus, reaction with 1-methyl-4-(4,4,5,5-tetramethyl-1,3,2-dioxaborolan-2-yl)-1H-pyrazole or cyclopropylboronic acid under Suzuki conditions yielded intermediates **17** and **18**. These thiomethyl derivatives were in turn oxidized to the corresponding sulfones

Scheme 2. Synthesis of Pyrido[3,4-*d*]pyrimidine Derivatives^a

Compound	R ¹	R ²
24a (24%)		
24b (17%)		
24c (48%)		
24d (43%)		

Compound	R ¹	R ²	Compound	R ¹	R ²
28a (29%)			28d (37%)		
28b (52%)	Me		28e (30%)		
28c (40%)					

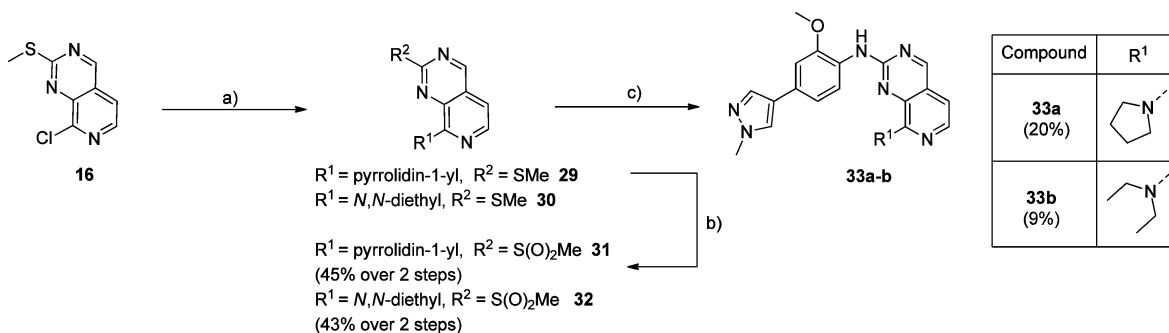
^aReagents and conditions: (a) 1-Methyl-4-(4,4,5,5-tetramethyl-1,3,2-dioxaborolan-2-yl)-1H-pyrazole, Na₂CO₃, Pd(dppf)Cl₂·CH₂Cl₂, THF/water, 65 °C (**17**); (b) cyclopropyl boronic acid, K₃PO₄, Pd(OAc)₂, PCy₃, toluene/water, 95 °C (**18**); (c) *m*-CPBA, CH₂Cl₂, rt; (d) *N*-(4-methoxyphenyl)formamide **21** or *N*-(2,4-dimethoxyphenyl)formamide **22**, DMSO, Cs₂CO₃, 100 °C (**24a,b**); (e) 2-methoxy-4-(1-methyl-1H-pyrazol-4-yl)aniline **23**, TFA, 1,1,1-trifluoroethanol, μW, 130 °C (**24c,d**); (f) ArNHCHO (**26a–e**), NaH, THF, rt; (g) 1-methyl-4-(4,4,5,5-tetramethyl-1,3,2-dioxaborolan-2-yl)-1H-pyrazole or phenyl boronic acid, Cs₂CO₃, Pd(PPh₃)₄, 1,4-dioxane/water, 100 °C. Reaction yields are in parentheses.

using *m*-CPBA and subsequently coupled with the required anilines or formamides to afford compounds **24a–d** (Scheme 2). In the majority of cases though, the order of events was reversed. Oxidation of 8-chloro-2-(methylthio)pyrido[3,4-*d*]pyrimidine **16** yielded the corresponding sulfone **25**,¹⁶ which was coupled with a series of formamides furnishing chloro-intermediates **27a–e** (Scheme 2). Final compounds **28a–e** were obtained by means of palladium-catalyzed Suzuki couplings with commercially available boronic acids or esters. Pyrido[3,4-*d*]pyrimidines **33a** and **33b** were prepared by direct substitution of amines on the 8-chloro-2-(methylthio)pyrido[3,4-*d*]pyrimidine building block **16** (Scheme 3). The resulting thiomethyl derivatives **29** and **30** were oxidized to the corresponding sulfones **31** and **32**

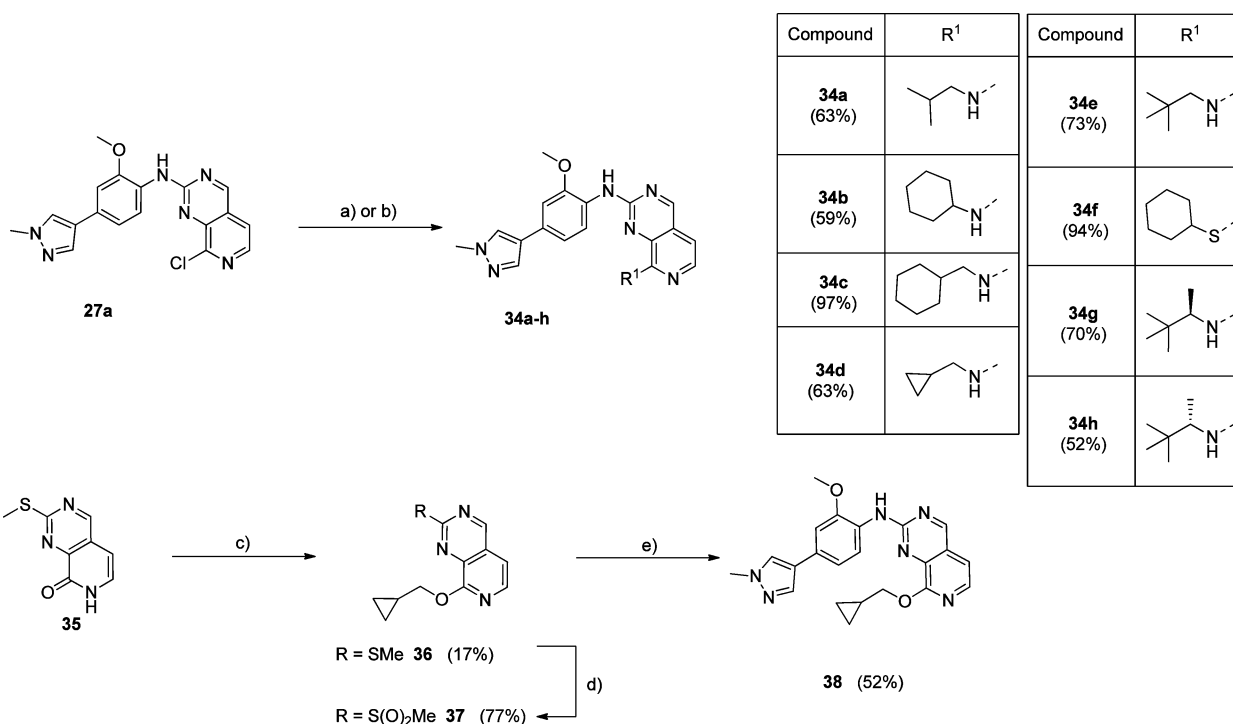
and subsequently coupled with the required formamides to afford final compounds **33a** and **33b**.

Pyrido[3,4-*d*]pyrimidines **34a–h** were prepared from intermediate **27a**¹⁶ by displacement using the appropriate nucleophiles (Scheme 4). In one instance the synthetic strategy involved the use of known pyridone **35**¹⁶ as a starting material: O-alkylation in the presence of base and bromomethyl cyclopropane gave intermediate **36**. Oxidation using *m*-CPBA and subsequent coupling with formamide **26a**¹⁶ afforded pyrido[3,4-*d*]pyrimidine **38** (Scheme 4).

In all cases, formamides and anilines were commercially available (**12**, **13**, **21**) or could be synthesized by means of standard transformations (**22**, **23**,¹⁷ and **26a–e**, see Exper-

Scheme 3. Functionalization of Pyrido[3,4-*d*]pyrimidine Core^a

^aReagents and conditions: (a) Amine, NMP, 80–135 °C; (b) *m*-CPBA, CH₂Cl₂, rt; (c) 2-methoxy-4-(1-methyl-1*H*-pyrazol-4-yl)aniline **23**, TFA, 1,2,3-trifluoroethanol, μ W, 130 °C. Reaction yields are in parentheses.

Scheme 4. Synthesis of Derivatives Containing 8-Position N, O, and S Substituents^a

^aReagents and conditions: (a) Amine, NMP, 80–135 °C (**34a–e, g, h**); (b) cyclohexyl thiol, K₂CO₃, DMF, rt (**34f**); (c) Ag₂CO₃, bromomethyl cyclopropane, CHCl₃, rt to 60 °C; (d) *m*-CPBA, CH₂Cl₂, rt; (e) *N*-(2-methoxy-4-(1-methyl-1*H*-pyrazol-4-yl)phenyl)formamide **26a**, NaH, THF, rt. Reaction yields are in parentheses.

imental section and Supporting Information for details). In every case, formylation was carried out by refluxing in formic acid.

RESULTS AND DISCUSSION

At the start of this work, relatively few inhibitors of MPS1 had been disclosed. In addition to our 1*H*-pyrrolo[3,2-*c*]pyridine series,⁷ we had identified and crystallized 1*H*-pyrazolo[4,3-*c*]pyridine **39**, a modestly potent hit, during an initial screening campaign. This compound showed low molecular weight (MW = 261) and acceptable ligand efficiency (L.E. = 0.43). The crystal structure of MPS1 in complex with **39** revealed that it binds in a complementary way to **4**, whereby the pyrazole moiety binds to the hinge region of the protein. The furan moiety occupies the same region as the carbamate in the 1*H*-pyrrolo[3,2-*c*]pyridine series. The phenyl ring and aniline moiety also occupy similar parts of the binding pocket (Figure 2).¹⁸ Based on these results,

we anticipated that **39** would represent a viable starting point for a second series but that extensive optimization of potency and selectivity would be required. In order to rapidly discover a new series, while utilizing previously gained SAR data, we merged the 1*H*-pyrrolo[3,2-*c*]pyridine scaffold with the screening hit **39** (Figure 3). Docking suggested that both the isoquinoline and pyrido[3,4-*d*]pyrimidine scaffolds could serve as hinge-binder elements for such a hybrid series (Figure 3). The isoquinoline scaffold had the advantage that proof-of-concept molecules could be rapidly prepared using precedented chemistry and commercially available building blocks. The pyrido[3,4-*d*]pyrimidine scaffold, on the other hand, was attractive from the point of view of novelty, the significantly lower lipophilicity, and the fact that it incorporated an additional pyridine nitrogen from screening hit **39**. This scaffold, however, required significant investigation into its synthesis.¹⁶ Our plan was thus to prepare a select number of

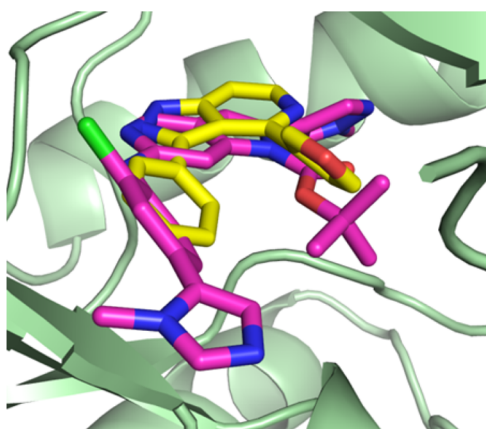


Figure 2. Superimposed crystal structure of MPS1 (pale green) bound to **1** (carbon atoms colored pink), extracted from PDB code 4C4J, onto the structure of MPS1 (not shown) bound to **39** (carbon atoms colored yellow), PDB code 5EHY, showing the complementary binding of the modestly potent hit **39** and MPS1 inhibitor **1** to the hinge region of MPS1.

proof-of-concept molecules based on the isoquinoline core and to expand into the less explored and more polar pyrido[3,4-*d*]pyrimidine series if the initial isoquinolines showed promising activity and ligand efficiency.

We used our biochemical MPS1 assay at 10 μM ATP concentration and an in-house electrochemiluminescence Meso Scale Discovery (MSD)-based cellular assay that measured autophosphorylation of ectopically expressed MPS1 in HCT116 cells.⁷ In addition, we routinely determined selectivity against CDK2 and Aurora A and B. We did not detect significant activity against either Aurora A or B throughout the series (see [Supporting Information](#)). Furthermore, as the IC_{50} values of our inhibitors approached the assay enzyme concentrations, and thus the limit of the dynamic range of our biochemical assay, we also determined the biochemical potency at a higher (1 mM) ATP concentration (*vide infra*). As stated above, our overall goal for this lead-finding effort was to show that potent (cellular $\text{IC}_{50} < 100$ nM) and selective compounds (CDK2/MPS1 K_i ratio > 100) could be obtained which exhibit lower molecular weight (around 450 Da) and improved ligand efficiency (L.E. in region of 0.35) compared with the 1*H*-pyrrolo[3,2-*c*]pyridine series. Moreover, our goal was to show robust activity in our PK/PD human tumor xenograft model.

The data for the initial set of compounds are summarized in [Table 1](#). The MPS1 inhibition for **14** was modest ($\text{IC}_{50} = 3.66$ μM , [Table 1](#)), but replacing the furan with a pyrazole (**15a**) not only lowered lipophilicity but also gave a 5-fold increase in potency ([Table 1](#)). Moreover, incorporating an additional methoxy group led to a significant gain in potency, and the IC_{50} of **15b** reached our goal for an initial proof-of-concept compound. As seen with the 1*H*-pyrrolo[3,2-*c*]pyridines,⁷ the latter greatly improved selectivity toward CDK2. The significant gain in potency can be ascribed to the interaction of the aniline's 2-methoxy substituent with a small hydrophobic pocket formed by Lys529, Ile531, Gln541, and Cys604.⁷ This pocket is not present in most other kinases including CDK2, explaining the beneficial effect on kinase selectivity.

Having achieved satisfactory potency and ligand efficiency (L.E. for **15b** = 0.36) by merging the 1*H*-pyrrolo[3,2-*c*]pyridine series and screening hit **39**, we investigated the less lipophilic pyrido[3,4-*d*]pyrimidine scaffold. Gratifyingly, 8-substituted 2-anilino-pyrido[3,4-*d*]pyrimidines proved to be more potent than their isoquinoline counterparts, reaching the double digit nanomolar range despite significantly lower calculated logP ([Table 1](#)). Isoquinoline **15b** along with pyrido[3,4-*d*]pyrimidines **24a** and **24b** were next tested in an MSD-based cellular assay. Both **15b** and **24b** showed only modest inhibition of the autophosphorylation of ectopically expressed MPS1 in HCT116 cells, most likely due to suboptimal biochemical potency. In the 1*H*-pyrrolo[3,2-*c*]pyridine series, introduction of a pyrazole substituent at the 4-position of the aniline caused a significant increase in biochemical and cellular potency.⁷ Gratifyingly, this structural modification also resulted in a further improvement in biochemical potency for the pyrido[3,4-*d*]pyrimidine series, with compound **24c** achieving a MPS1 $\text{IC}_{50} = 0.008$ μM and a cellular P-MPS1 $\text{IC}_{50} = 0.604$ μM ([Table 1](#)).

We solved the crystal structure of MPS1 in complex with isoquinoline **15b** and pyrido[3,4-*d*]pyrimidine **24b** ([Figure 4](#)). The two structures overlaid very well with the crystal structure of **1** ([Figure 4A and B](#)), binding to the hinge region through the same motif as seen with the 1*H*-pyrrolo[3,2-*c*]pyridines. This reinforced our initial hypothesis that merging the 1*H*-pyrrolo[3,2-*c*]pyridine series and **39** would give a suitable starting point for an additional series of inhibitors. The aniline portion of all compounds overlaps as well as the 5-position and 8-position substituents of the isoquinolines and pyrido[3,4-*d*]pyrimidines,

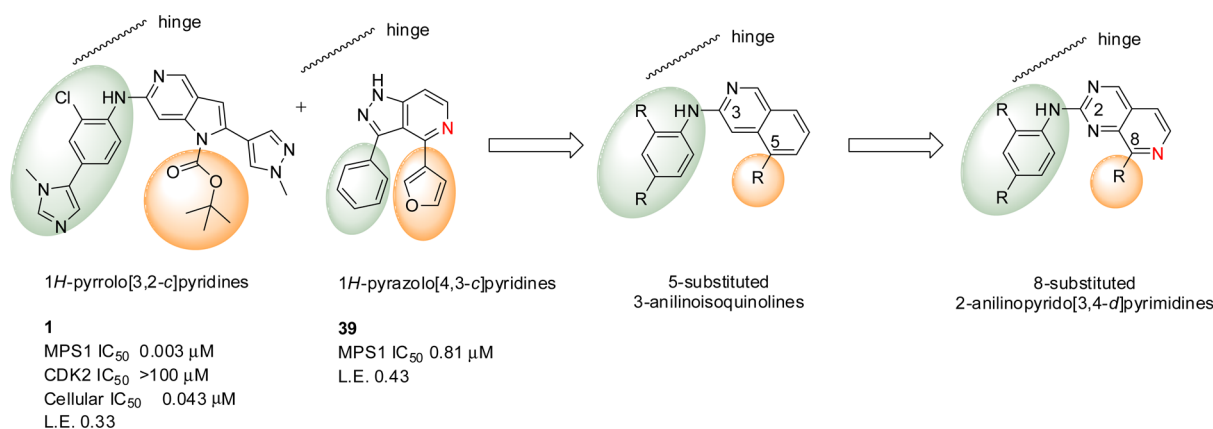


Figure 3. Hybridization strategy for the development of a novel chemical series of inhibitors of MPS1, from previously reported inhibitor **1** and screening hit **39**.

Table 1. Biochemical and Cellular Data for Initial Proof-of-Concept Isoquinolines (14, 15a, 15b) and Pyrido[3,4-*d*]pyrimidines (24a–c)^a

Compd	Structure	Biochemical IC ₅₀ (μM)		Cellular P-MPS1 IC ₅₀ (μM)	AlogP
		MPS1	CDK2		
14		3.66 (1.36, 5.95)	31.1	-	4.57
15a		0.66±0.08	1.22 (1.54, 0.91)	-	3.83
15b		0.099±0.064	85.5	2.77 (1.93, 3.61)	3.81
24a		0.14±0.05	0.089±0.014	> 10	2.89
24b		0.046±0.018	1.54±0.30	4.84±3.29	2.87
24c		0.008±0.002 ^b	1.28±0.41	0.60±0.16	3.06

^aResults are mean (±SD) for $n \geq 3$ or mean values of two independent determinations with individual determinations in parentheses or samples run $n = 1$. “P-MPS1” indicates an electrochemiluminescence MSD-based cellular assay that measured autophosphorylation of ectopically expressed MPS1 in HCT116 cells. ^bPotency at the lower limit of the dynamic range of the Caliper assay run at 10 μM ATP concentration. IC₅₀ value is likely to be lower than that quoted.

respectively, occupying the same region as the carbamate group of **1**. Of note is the difference in conformation for **15b** and **24b** (Figure 4C and D). The introduction of two extra nitrogen atoms into the aromatic ring, and thus removal of two hydrogen atoms, results in a much more planar structure for the pyrido[3,4-*d*]pyrimidine **24b**. We measured the dihedral angles for both of these compounds: isoquinoline **15b** exhibits a dihedral angle of 98° and pyrido[3,4-*d*]pyrimidine **24b** exhibits a dihedral angle of -20° (Figure 4D). The more coplanar conformation of pyrido[3,4-*d*]pyrimidines mirrors the coplanar conformation of the carbamate function of **1** and is likely to be at least partially responsible for the improved activity seen with the much less lipophilic pyrido[3,4-*d*]pyrimidines. Based on these crystal structures, we had confidence that with further optimization we would achieve potent and selective pyrido[3,4-*d*]pyrimidine based inhibitors of MPS1.

Through our hybridization strategy and exploration of the pyrido[3,4-*d*]pyrimidine scaffold, we had achieved a potent inhibitor (**24c**, MPS1 IC₅₀ = 0.008 μM) and for the first time reached significant levels of cellular inhibition with IC₅₀ values below 1 μM. Compound **24c** represented a promising starting point for further optimization of this compound into a novel series of MPS1 inhibitors.

Since our initial goal was to show target modulation in a human tumor xenograft model in mice, we investigated the stability of **24c** in mouse liver microsomes. Unfortunately, **24c** showed high turnover (MLM = 73% following 30 min incubation) and was not suitable for in vivo experiments. Metabolite ID studies suggested loss of a methyl group, and we suspected that the methoxy aniline substituent was the most likely site of demethylation. This methoxy group was important for both potency and selectivity. After consideration of the X-ray crystal structures we had in hand, suggesting that larger substituents at this position would be tolerated, we prepared and tested a series of compounds in which this putative metabolic soft spot was replaced with similar moieties (Table 2). The majority of these compounds showed higher IC₅₀ values than **24c** with the exception of the ethoxy derivative **28c**, which achieved comparable potency, while exhibiting significantly improved CDK2 selectivity (>28 fold improvement over **24c**) and MLM stability (MLM = 45%). This increase in selectivity is likely due to the fact that the aniline 2-position substituent occupies a small lipophilic pocket present in MPS1, mentioned previously, consisting of Lys529, Ile531, Gln541 and the gatekeeper+2 residue Cys604. This pocket is not available in CDK2 due to the presence of the bulkier gatekeeper residue Phe82. The larger 2-

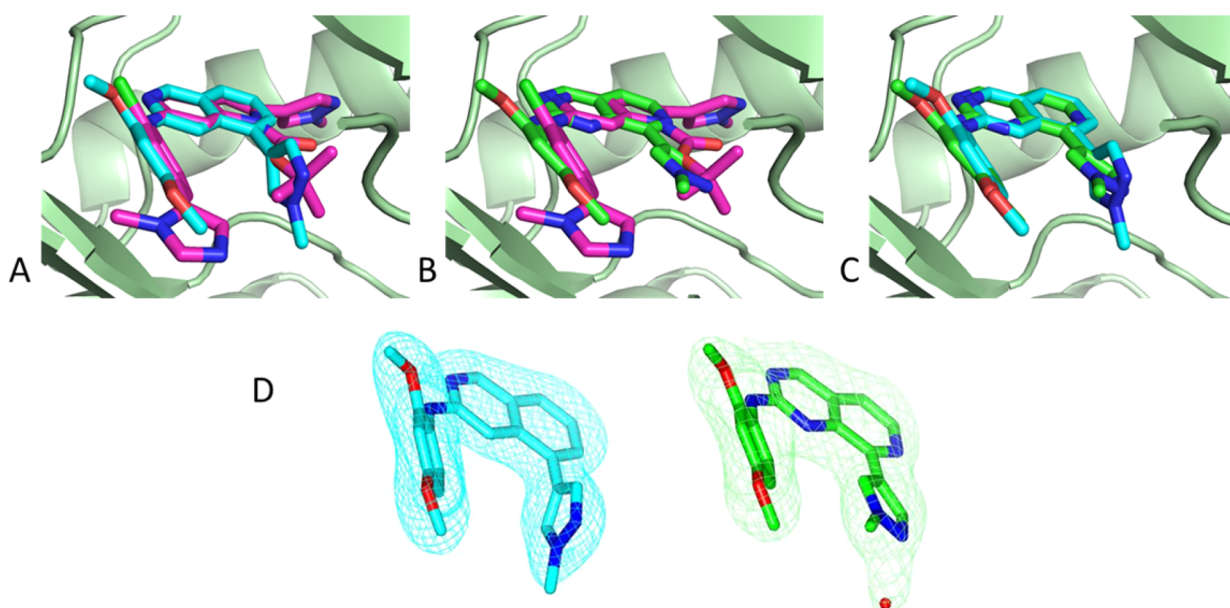


Figure 4. (A) Superimposed crystal structure of MPS1 (pale green) bound to **1** (carbon atoms colored pink), extracted from PDB code 4C4J, onto the structure of MPS1 (not shown) bound to **15b** (carbon atoms colored cyan), PDB code 5EI6. (B) Superimposed crystal structure of MPS1 (pale green) bound to **1** (carbon atoms colored pink), extracted from PDB code 4C4J, onto the structure of MPS1 (not shown) bound to **24b** (carbon atoms colored green), PDB code 5EI2. (C) Superimposed crystal structure of MPS1 (pale green) bound to **15b** (carbon atoms colored cyan), extracted from PDB code 5EI6, onto the structure of MPS1 (not shown) bound to **24b** (carbon atoms colored green), PDB code 5EI2, showing the extent of the conformational difference between the isoquinoline and pyrido[3,4-*d*]pyrimidine scaffolds. (D) Side-by-side view of compound **15b** (carbon atoms colored cyan) and **24b** (carbon atoms colored green) showing the difference in angle of the *N*-methylpyrazole group. $2F_o - F_c$ density contoured at 1σ is overlaid and displayed in the same color as the respective compound carbon atom color. A water molecule interacting with compound **24b** is also displayed as a red sphere. **15b** exhibits a dihedral angle of 98° , and **24b** exhibits a dihedral angle of -20° .

position ethoxy substituent (**28c**) clashes with the CDK2 gatekeeper+2 residue, resulting in a better selectivity window than is seen for the methoxy derivative **24c**.

Unfortunately, **28c** was 5-fold less active in the cellular assay, which given the similar biochemical potency and physicochemical properties was difficult to rationalize. While we regarded the ethoxy as a valuable alternative for the methoxy group, with significantly improved selectivity and reduced risk of reactive intermediate formation through metabolic dealkylation, we decided to maintain the methoxy in place due to the improved cellular activity. Instead, we looked to improve the metabolic stability through modification at the 8-position of the pyrido[3,4-*d*]pyrimidine scaffold. We hypothesized that by introducing diverse substituents at this position of the scaffold, the molecular recognition of the compounds by metabolic enzymes would be affected leading to increased stability.

In order to address these aspects we used the structural information gathered on pyrido[3,4-*d*]pyrimidine **24c**. The crystal structure of this inhibitor showed that the 8-position pyrazole group binds to a hydrophobic pocket formed by Ile531, Val539, Met671, and Pro673 (Figure 5A). This is the same pocket that is occupied by the carbamate group of **1** and is sufficiently large to accommodate a variety of hydrophobic groups (Figure 5B). It is also of note that the crystal structure of MPS1 in complex with **24c** shows ordering of the activation loop of MPS1, as is seen with **1**.⁷ We thus prepared and tested a small set of compounds with different pyrazole replacements including a saturated pyrrolidine ring.

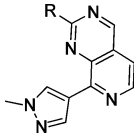
The data for these compounds are summarized in Table 3. The phenyl-substituted derivative (**28a**) showed comparable potency in the biochemical and cellular assay and, despite higher lipophilicity, improved microsomal stability. The cyclopropyl

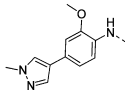
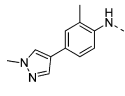
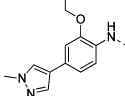
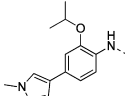
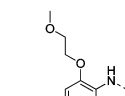
derivative **24d** lost considerable activity, possibly due to the fact that this group is too small to engage in significant hydrophobic interactions. Interestingly, replacement of the pyrazole with a saturated pyrrolidine (**33a**) led to an equipotent compound in the biochemical assay. All compounds showed selectivity against CDK2 (CDK2/MPS1 ratio >80).

Of the compounds presented in Table 3, we considered the pyrrolidine derivative (**33a**) as the most promising for further optimization. A saturated moiety offered more possibilities to optimize the three-dimensional hydrophobic interactions in this subpocket compared with an aromatic ring where substituents can only be placed in the plane of the ring. Furthermore, increasing the number of sp^3 centers has been suggested as a general approach to improve solubility and drug-like properties.¹⁹ We thus prepared a series of compounds with a saturated substituent in this position.

Importantly, since the IC_{50} values of many compounds were now approaching the enzyme concentration and thus the limit of the dynamic range of the biochemical assay, we complemented the MPS1 kinase assay at $10\ \mu\text{M}$ ATP with testing at $1\ \text{mM}$ ATP. It has been demonstrated that increasing the ATP concentration shifts the IC_{50} values of ATP competitive inhibitors to higher values, therefore increasing the dynamic range of the assay.²⁰ Due to the differing ATP concentrations in the high ATP Caliper assay and the CDK2 assay ($1\ \text{mM}$ MPS1 vs $10\ \mu\text{M}$ CDK2), the assays were no longer directly comparable. For this reason, we used the Cheng–Prusoff equation to calculate the K_i values²¹ and, in turn, used these values to determine the selectivity window.

Compound **33b**, incorporating a diethylamine substituent, was significantly (6-fold) less potent in the $1\ \text{mM}$ ATP Caliper assay than the pyrrolidine **33a** (Table 4). This is likely due to a

Table 2. Biochemical, Cellular, And Mouse Microsomal Turnover Data for Compounds Bearing Alternative Aniline Substituents^a


Compd	R	Biochemical IC ₅₀ (μM)		Cellular P-MPS1 IC ₅₀ (μM)	MLM % (30 min)	AlogP
		MPS1	CDK2			
24c		0.008±0.002 ^b	1.28±0.41	0.60±0.16	73	3.06
28b		0.024±0.014	0.38 (0.17, 0.59)	2.54±0.79	63	3.56
28c		0.010±0.003 ^b	> 45	2.64±0.34	45	3.41
28d		0.049 (0.067, 0.030)	>10	-	45	3.78
28e		0.14±0.05	-	-	59	2.93

^aResults are mean (±SD) for $n \geq 3$, or mean values of two independent determinations with individual determinations in parentheses or samples run $n = 1$. "P-MPS1" indicates an electrochemiluminescence MSD-based cellular assay that measured autophosphorylation of ectopically expressed MPS1 in HCT116 cells. ^bPotency at the lower limit of the dynamic range of the Caliper assay run at 10 μM ATP concentration. IC₅₀ value is likely to be lower than that quoted.

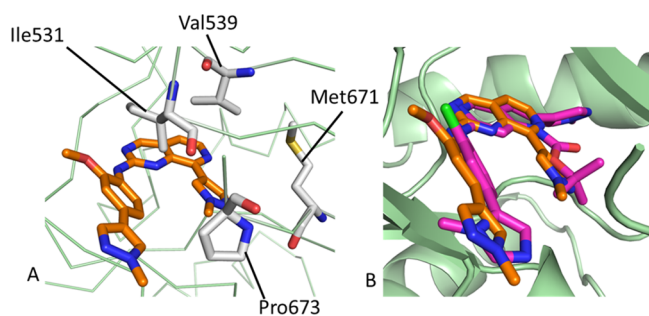


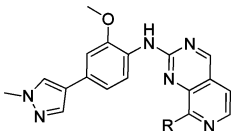
Figure 5. (A) Crystal structure of MPS1 (pale green) bound to 24c (carbon atoms colored orange), extracted from PDB code 5E18, showing residues (Ile531, Val539, Met671, and Pro673) present in the hydrophobic pocket occupied by 8-position pyrazole. (B) Superimposed crystal structure of MPS1 (pale green) bound to 24c (carbon atoms colored orange), extracted from PDB code 5E18, onto the structure of MPS1 (not shown) bound to 1 (carbon atoms colored pink), PDB code 4C4J, showing that this is the same pocket occupied by the carbamate group of 1 (carbon atoms colored pink).

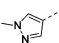
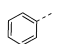

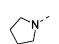
higher free energy penalty when binding to the target for this less constrained compound. Gratifyingly, several amine substituents (34b, d, and e) not only showed comparable biochemical

potency but also improved microsomal stability, now in an acceptable range of 30% turnover.

Since saturated amines were well tolerated in this position, we next prepared and tested derivatives in which the alkyl groups were linked through a sulfur or oxygen atom (34f and 38). Remarkably, both lost significant activity (at least 10-fold) compared to the corresponding amine derivatives 34b and 34d. It is difficult to reconcile the pronounced loss of activity of compounds 34f and 38 with the wide range of both primary and secondary amines that are tolerated. Computational conformational analysis did not suggest a significant difference in the conformational preference of the oxygen and sulfur-linked substituents compared to the amine substituents. Furthermore, analysis of the available crystal structure did not support the hypothesis that this difference may be driven by different hydrogen-bond pattern, e.g., to water molecules.

Several amino-substituted compounds did however show potent IC₅₀ values suggesting significant scope for further modifications. The neopentyl derivative 34e was particularly promising due to its cellular potency combined with selectivity and improved mouse microsomal stability. As is apparent from the MPS1 IC₅₀ at 1 mM ATP, it was also the most potent derivative in this series.

Table 3. Biochemical, Cellular, And Mouse Microsomal Turnover Data for Compounds Bearing Alternative 8-Position Substituents^a


Compd	R	Biochemical IC ₅₀ (μM)		Cellular P-MPS1 IC ₅₀ (μM)	MLM % (30 min)	AlogP
		MPS1	CDK2			
24c		0.008±0.002 ^b	1.28±0.41	0.60±0.16	73	3.06
28a		0.018±0.006	> 100	0.48±0.10	40	4.41
24d		0.11±0.02	9.74 (12.55, 6.93)	7.81±6.18	51	3.50
33a		0.010±0.003 ^b	2.83±0.77	2.20±1.71	64	3.62

^aResults are mean (±SD) for $n \geq 3$, or mean values of two independent determinations with individual determinations in parentheses or samples run $n = 1$. "P-MPS1" indicates an electrochemiluminescence MSD-based cellular assay that measured autophosphorylation of ectopically expressed MPS1 in HCT116 cells. ^bPotency at the lower limit of the dynamic range of the Caliper assay run at 10 μM ATP concentration. IC₅₀ value is likely to be lower than that quoted.

We solved the structure of neopentyl **34e** bound into MPS1 (Figure 6). Figure 6 shows that the bulkier, more hydrophobic neopentyl substituent of **34e** addresses the hydrophobic pocket first mentioned in Figure 5A to a greater extent than the pyrazole substituent of **24c**. We hypothesized that an additional increase in potency could be achieved by further increasing the bulk of the hydrophobic substituent.

We thus followed up by synthesizing the two enantiomers **34g** and **34h** which differ from the neopentyl **34e** by an additional methyl group (Table 5). The (*S*)-enantiomer (**34h**) particularly, translated into an additional gain in biochemical and cellular potency compared with neopentyl derivative **34e**, achieving cellular modulation of MPS1 in the sub-100 nM range (Table 5). **34h** showed sufficient selectivity over CDK2 and very good microsomal stability (MLM = 27%).

With **34h** we had achieved our initial potency goal in the biochemical and cellular assay. Especially considering its moderate molecular weight of 432 Da, **34h** represented an extremely potent MPS1 inhibitor with an IC₅₀ = 0.020 μM at 1 mM ATP (corresponding to a K_i of 0.0002 μM)²¹ and a GI₅₀ value in HCT116 cells of 0.16 μM. Furthermore, the combined SAR suggested significant scope for additional modifications to further optimize the series. This pyrido[3,4-*d*]pyrimidine (**34h**) was selective over CDK2 (CDK2/MPS1 K_i ratio > 1000),²¹ Aurora A and B (Table S1), and PLK1 (IC₅₀ > 100 μM) as well as against a wide panel of kinases (Tables S2–S4). Pyrido[3,4-*d*]pyrimidine **34h** inhibited a small number of kinases, namely TNK2, JNK1, JNK2, and LRRK at >80% at 1 μM. JNK1 and JNK2 are considered to be structurally related to MPS1, so follow up IC₅₀ values were obtained (JNK1 IC₅₀ = 0.11 μM, JNK2 IC₅₀

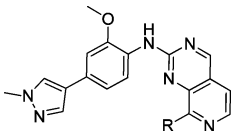
= 0.22 μM), showing that **34h** was selective for MPS1 over JNK1 and JNK2 by 100- and 200-fold, respectively.

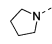
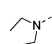
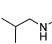
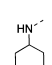
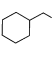
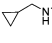
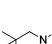
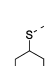
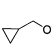
Next we profiled **34h** against a panel of cell lines (Table 6). As expected for an MPS1 inhibitor, **34h** showed potent growth inhibition for all cancer cell lines but importantly a significantly higher GI₅₀ for the nontransformed line PNT2.

34h did not inhibit CYP or hERG (Tables S5 and S6). Importantly, pyrido[3,4-*d*]pyrimidine **34h**, showed low turnover in mouse and rat liver microsomes (27 and 24%, after 30 min incubation, respectively), and we progressed the compound to mouse and rat PK experiments, despite a 70% turnover in human liver microsomes, in order to evaluate its suitability for proof of mechanism in vivo experiments. **34h** showed moderate clearance (28 and 24 mL/min/kg in mouse and rat, respectively) and high oral bioavailability (68 and 100% in mouse and rat, respectively) with moderate to high volumes of distribution (Table 7).

We thus performed a 3 day pharmacokinetic/pharmacodynamic (PK/PD) study to determine whether biomarker modulation could be achieved in vivo. MPS1 inhibition results in premature exit of cells from mitosis,^{10e} and we therefore chose the mitotic marker phospho-histone H3 as a readout. Histone H3 is specifically phosphorylated at Ser 10 during mitosis.²² Gratifyingly, oral administration of 100 mg/kg of **34h** b.i.d. for 3 days to mice bearing HCT116 human colon carcinoma xenografts caused a reduction of the phospho-histone H3 levels compared with vehicle control treated animals at 2 and 6 h, consistent with MPS1 inhibition (Figure 7).

Compound **34h** fulfilled all of the criteria we had initially set and compared favorably with our best-in-class 1*H*-pyrrolo[3,2-*c*]pyridine (**1**). Particularly, **34h** was devoid of CYP inhibition, did not require an acid labile Boc group for biochemical and

Table 4. Biochemical, Cellular, And Mouse Microsomal Turnover Data for Compounds Bearing a Saturated Substituent at the 8-Position^a


Compd	R	Biochemical activity (μM)				Cellular activity (μM)		MLM % (30 min)	AlogP / L.E.	
		MPS1 IC ₅₀	MPS1 (1 mM ATP)		CDK2 IC ₅₀	P-MPS1 IC ₅₀	HCT 116 GI ₅₀			
			IC ₅₀	K _i						K _i
33a		0.010 ± 0.003 ^b	0.33 ± 0.18	0.0033	2.83 ± 0.77	1.42	2.20 ± 1.71	0.47 (0.46, 0.47)	64	3.62/ 0.37
33b		0.062 ± 0.010	>1 (n=2)	-	-	-	-	-	-	3.86/ 0.34
34a		0.016 ± 0.008 ^b	0.37 ± 0.15	0.0037	0.85 ± 0.40	0.43	0.65 ± 0.17	1.1	66	4.00/ 0.36
34b		0.012 ± 0.005 ^b	0.13 (0.18, 0.08)	0.0013	0.19 ± 0.04	0.10	0.22 ± 0.06	0.12 (0.10, 0.14)	22	4.67/ 0.35
34c		0.046 ± 0.015	>1 (n=2)	-	-	-	-	-	-	5.00/ 0.31
34d		0.011 ± 0.004 ^b	0.28 ± 0.16	0.0028	1.08 ± 0.69	0.54	0.43 ± 0.06	0.32	33	3.63/ 0.37
34e		0.018 ± 0.017 ^b	0.045 ± 0.023	0.0005	0.45 ± 0.21	0.23	0.14 (0.15, 0.14)	0.34 (0.24, 0.43)	31	4.27/ 0.35
34f		0.25 ± 0.13	-	-	>10 0	-	-	-	-	5.40/ 0.29
38		0.15 (0.10, 0.20)	-	-	-	-	-	-	-	3.80/ 0.32

^aResults are mean (\pm SD) for $n \geq 3$, or mean values of two independent determinations with individual determinations in parentheses or samples run $n = 1$. "P-MPS1" indicates an electrochemiluminescence MSD-based cellular assay that measured autophosphorylation of ectopically expressed MPS1 in HCT116 cells. "HCT116 GI₅₀" indicates a cell proliferation assay carried out by colorimetric 3-(4,5-dimethylthiazol-2-yl)-2,5-diphenyltetrazolium bromide (MTT) assay in HCT116 cells. ^bPotency at the lower limit of the dynamic range of the Caliper assay run at 10 μM ATP concentration. IC₅₀ value is likely to be lower than that quoted.

cellular potency, and showed excellent overall selectivity. Its physicochemical properties (AlogP = 4.65 and MW = 432) made **34h** a better starting point for further optimization especially given that we had already achieved the targeted potency. Surprisingly, given that it represented a pyrimidine-based kinase scaffold, the 2-amino pyrido[3,4-*d*]pyrimidine

chemotype was relatively unexplored when we initiated this work, with only one published kinase patent application in the public domain.²³ Our previously published chemical route¹⁶ facilitated the synthesis of a large range of derivatives as well as upscaling of advanced derivatives. We thus nominated **34h** as an advanced lead compound.

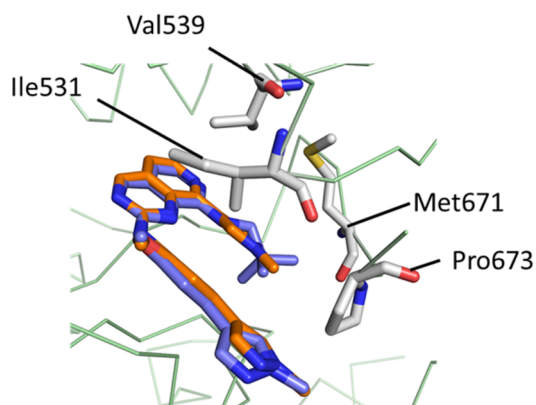


Figure 6. Superimposed crystal structure of MPS1 (pale green) bound to **24c** (carbon atoms colored orange), extracted from PDB code SEI8, onto the structure of MPS1 (not shown) bound to **34e** (carbon atoms colored blue), PDB code SEH0, showing the hydrophobic pocket formed by Ile531, Val539, Met671, and Pro673. The bulkier neopentyl substituent of **34e** addresses the pocket to a greater extent than the pyrazole substituent of **24c**.

CONCLUSIONS

By merging two distinct chemical series, namely 1*H*-pyrrolo[3,2-*c*]pyridines and 1*H*-pyrazolo[4,3-*c*]pyridines, we successfully fulfilled our aim to discover a new class of MPS1 inhibitors that did not require an acid labile Boc group for potent inhibition. The pyrido[3,4-*d*]pyrimidine core was unprecedented for kinases,¹⁶ and our structure guided optimization resulted in potent MPS1 inhibitors of substantially reduced size and lipophilicity compared with the parent 1*H*-pyrrolo[3,2-*c*]-

Table 6. GI₅₀ Values for **34h** in 3 Day MTT Assay Carried out on Panel of Cell Lines^a

origin	cell line	GI ₅₀ (μM)
colon	SW620	0.065
head and neck	CAL27	0.23
breast	CAL51	0.068
pancreatic	Miapaca-2	0.25
ovarian	RMG1	0.110
prostate	PNT2	3.95

^aGI₅₀ indicates a cell proliferation assay carried out by colorimetric 3-(4,5-dimethylthiazol-2-yl)-2,5-diphenyltetrazolium bromide (MTT) assay in a panel of cell lines.

pyridines. Moreover, our optimized compound **34h** was devoid of CYP inhibition and proved to be extremely potent in the MPS1 biochemical assay with the ability to target this kinase in cells and to induce significant growth inhibition at nanomolar concentrations. A screen against a large sample of the human kinome revealed a high level of selectivity, especially with regard to mitotic kinases. Most importantly, pyrido[3,4-*d*]pyrimidine **34h** showed a satisfactory pharmacokinetic profile in rodents and effectively inhibited MPS1 activity in vivo.

Optimization of the remaining issues associated with **34h**, in particular HLM instability and plasma protein binding, as well as the investigation of advanced compounds in combination efficacy models, is ongoing and the results will be reported in due course.

Table 5. Biochemical, Cellular, And Mouse Microsomal Turnover Data for Enantiomers **34g** and **34h**^a

Compd	R	Biochemical activity (μM)				Cellular activity (μM)		MLM % (30 min)	AlogP/L.E.
		MPS1 (1 mM ATP)		CDK2		P-MPS1 IC ₅₀	HCT 116 GI ₅₀		
		IC ₅₀	K _i	IC ₅₀	K _i				
34e		0.018 ± 0.017 ^b	0.045 ± 0.023	0.0005	0.45 ± 0.21	0.14 (0.15, 0.14)	0.34 (0.24, 0.43)	31	4.27/0.35
34g		0.022 ± 0.014 ^b	0.42 ± 0.23	0.0042	0.47 ± 0.25	0.19 ± 0.08	0.22	25	4.65/0.33
34h		0.011 ± 0.005 ^b	0.020 ± 0.013	0.0002	0.56 (0.71, 0.41)	0.059 ± 0.022	0.16 (0.15, 0.16)	27	4.65/0.35

^aResults are mean (±SD) for $n \geq 3$, or mean values of two independent determinations with individual determinations in parentheses or samples $n = 1$. "P-MPS1" indicates an electrochemiluminescence MSD-based cellular assay that measured autophosphorylation of ectopically expressed MPS1 in HCT116 cells. "HCT116 GI₅₀" indicates a cell proliferation assay carried out by colorimetric 3-(4,5-dimethylthiazol-2-yl)-2,5-diphenyltetrazolium bromide (MTT) assay in HCT116 cells. ^bPotency at the lower limit of the dynamic range of the Caliper assay run at 10 μM ATP concentration. IC₅₀ value is likely to be lower than that quoted.

Table 7. Mouse and Rat Blood Pharmacokinetics of 34h at 5 mg/kg iv and po

species	$t_{1/2}$ (h)	Cl (mL/min/kg)	C _{max} _{po} (nmol/L)	AUC _{po} (nmol-h/L)	PPB (%)	V _{ss} (L/kg)	F (%)
mouse	8.2	28	770	4800	99.98	14.7	68
rat	2.5 ^a	24	560	9300	99.97	4.64	100

^aOnly detected to 4 h.

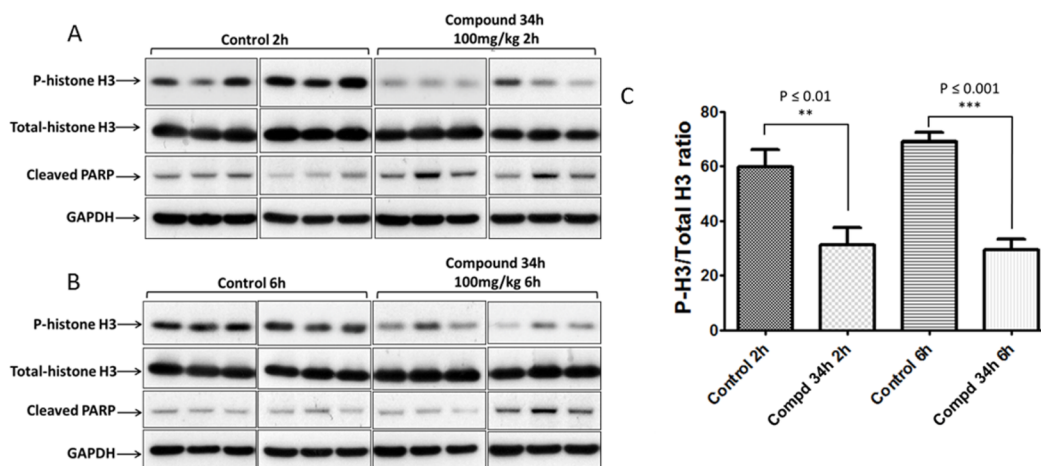


Figure 7. (A,B) Representative immunoblots of phospho-histone H3 showing dose-dependent PD modulation in HCT116 human tumor xenografts, following 100 mg/kg b.i.d. dosing of 34h for 3 consecutive days. Total histone H3, cleaved poly ADP ribose polymerase (PARP, a measure of apoptosis) and glyceraldehyde 3-phosphate dehydrogenase (GAPDH, for protein loading) are also shown. (C) Phospho-histone H3 versus total histone H3 ratio for control and treated samples at 2 and 6 h after last dose. Asterisks show statistically significant differences from control groups as determined by one-way ANOVA.

EXPERIMENTAL SECTION

General Chemistry Information. Starting materials, reagents, and solvents for reactions were reagent grade and used as purchased. Chromatography solvents were HPLC grade and were used without further purification. Thin-layer chromatography analysis was performed using silica gel 60 F-254 thin-layer plates. Flash column chromatography was carried out using columns prepacked with 40–63 μ m silica. Microwave-assisted reactions were carried out using a Biotage Initiator microwave system. LCMS and HRMS analyses were performed on a HPLC system with diode array detector operating at 254 nm, fitted with a reverse-phase 50 \times 4.6 mm column at a temperature of 22 $^{\circ}$ C, connected to a time of flight mass spectrometer (ESI). The following solvent system, at a flow rate of 2 mL/min, was used: Solvent A: methanol; solvent B: 0.1% formic acid in water. Gradient elution was as follows: 1:9 (A:B) to 9:1 (A:B) over 2.5 min, 9:1 (A:B) for 1 min then reversion back to 1:9 (A:B) over 0.3 min, 1:9 (A:B) for 0.2 min. 1 H NMR spectra were recorded on a Bruker Avance 500 MHz spectrometer using an internal deuterium lock. NMR data is given as follows: chemical shift (δ) in ppm, multiplicity, coupling constants (J) given in Hz and integration. The purity of final compounds was determined by HPLC as described above and is \geq 95% unless specified otherwise.

Compounds 2-methoxy-4-(1-methyl-1H-pyrazol-4-yl)aniline (**23**),¹⁷ 8-chloro-2-(methylsulfonyl)pyrido[3,4-d]pyrimidine (**25**),¹⁶ N-(2-methoxy-4-(1-methyl-1H-pyrazol-4-yl)phenyl)formamide (**26a**),¹⁶ 8-chloro-N-(2-methoxy-4-(1-methyl-1H-pyrazol-4-yl)phenyl)pyrido[3,4-d]pyrimidin-2-amine (**27a**),¹⁶ and 2-(methylthio)pyrido[3,4-d]pyrimidin-8(7H)-one (**35**)¹⁶ were synthesized using previously published procedures.

3-Chloro-5-(furan-2-yl)isoquinoline 10. A suspension of 5-bromo-3-chloroisoquinoline **9** (58 mg, 0.24 mmol), furan-2-ylboronic acid (32 mg, 0.29 mmol), and Pd(dppf)Cl₂·CH₂Cl₂ (20 mg, 0.024 mmol) in DME (0.5 mL) and sodium carbonate (2 M, 0.24 mL) was heated to 105 $^{\circ}$ C under microwave irradiation for 1 h. The mixture was concentrated onto silica gel and purified by flash column chromatography (0–50% EtOAc in cyclohexane) to give the title compound (41 mg, 75%). HRMS (ESI) m/z calcd for C₁₃H₉ClNO (M + H) 230.0367, found 230.0343. 1 H NMR (500 MHz, CDCl₃) δ 9.09 (s, 1H), 8.33 (s, 1H),

7.99–7.90 (m, 2H), 7.71–7.55 (m, 2H), 6.79 (dd, J = 3.4, 0.6 Hz, 1H), 6.62 (dd, J = 3.4, 1.8 Hz, 1H).

3-Chloro-5-(1-methyl-1H-pyrazol-4-yl)isoquinoline 11. A suspension of 5-bromo-3-chloroisoquinoline **9** (300 mg, 1.24 mmol), 1-methyl-4-(4,4,5,5-tetramethyl-1,3,2-dioxaborolan-2-yl)-1H-pyrazole (309 mg, 1.49 mmol), and Pd(dppf)Cl₂·CH₂Cl₂ (105 mg, 0.124 mmol) in DME (2.5 mL) and sodium carbonate (2 M, 1.24 mL) was heated to 105 $^{\circ}$ C under microwave irradiation for 1.5 h. The mixture was concentrated onto silica gel and purified by flash column chromatography (0–100% EtOAc in cyclohexane) to give the title compound (324 mg, quant.). HRMS (ESI) m/z calcd for C₁₃H₁₁ClN₃ (M + H) 244.0636, found 244.0639. 1 H NMR (500 MHz, CDCl₃) δ 9.08 (s, 1H), 7.96 (s, 1H), 7.90 (d, J = 8.1 Hz, 1H), 7.73 (s, 1H), 7.67–7.55 (m, 3H), 4.05 (s, 3H).

5-(Furan-2-yl)-N-(4-methoxyphenyl)isoquinolin-3-amine 14. A suspension of 3-chloro-5-(furan-2-yl)isoquinoline **10** (41 mg, 0.18 mmol), 4-methoxyaniline **12** (29 mg, 0.23 mmol), cesium carbonate (204 mg, 0.626 mmol), ^tBuXPhos (30 mg, 0.071 mmol), Pd₂(dba)₃ (16 mg, 0.018 mmol), and ^tBuOH (3% H₂O) (1 mL) was heated to 80 $^{\circ}$ C under microwave irradiation for 3 h. The mixture was concentrated onto silica gel and purified by flash column chromatography (0–100% EtOAc in cyclohexane) to give the title compound (10 mg, 18%). HRMS (ESI) m/z calcd for C₂₀H₁₇N₂O₂ (M + H) 317.1285, found 317.1282. 1 H NMR (500 MHz, CDCl₃) δ 8.95 (s, 1H), 7.84–7.75 (m, 2H), 7.61 (s, 1H), 7.57 (s, 1H), 7.58–7.25 (m, 3H), 7.17–6.90 (m, 2H), 6.77–6.60 (m, 2H), 6.54 (dd, J = 3.3, 1.8 Hz, 1H), 3.85 (s, 3H).

N-(4-Methoxyphenyl)-5-(1-methyl-1H-pyrazol-4-yl)isoquinolin-3-amine 15a. A suspension of 3-chloro-5-(1-methyl-1H-pyrazol-4-yl)isoquinoline **11** (55 mg, 0.23 mmol), 4-methoxyaniline **12** (36 mg, 0.29 mmol), cesium carbonate (257 mg, 0.789 mmol), ^tBuXPhos (38 mg, 0.090 mmol), Pd₂(dba)₃ (21 mg, 0.023 mmol), and ^tBuOH (3% H₂O) (1 mL) was heated to 80 $^{\circ}$ C under microwave irradiation for 1.5 h. The mixture was concentrated onto silica gel and purified by flash column chromatography (0–100% EtOAc in cyclohexane) to give the title compound (6 mg, 8%). HRMS (ESI) m/z calcd for C₂₀H₁₉N₄O (M + H) 331.1553, found 331.1546. 1 H NMR (500 MHz, CDCl₃) δ 8.95 (s, 1H), 7.75 (d, J = 8.2 Hz, 1H), 7.68 (s, 1H), 7.52 (s, 1H), 7.50–7.46 (m,

2H), 7.31–7.21 (m, 3H), 7.03–6.89 (m, 2H), 6.48 (s, 1H), 3.98 (s, 3H), 3.83 (s, 3H).

***N*-(2,4-Dimethoxyphenyl)-5-(1-methyl-1H-pyrazol-4-yl)-isoquinolin-3-amine 15b.** A suspension of 3-chloro-5-(1-methyl-1H-pyrazol-4-yl)isoquinoline **11** (55 mg, 0.23 mmol), 2,4-dimethoxyaniline **13** (45 mg, 0.29 mmol), cesium carbonate (257 mg, 0.789 mmol), ^tBuXPhos (38 mg, 0.090 mmol), Pd₂(dba)₃ (21 mg, 0.023 mmol), and ^tBuOH (3% H₂O) (1 mL) was heated to 80 °C under microwave irradiation for 1.5 h and then to 100 °C for 1.5 h. The mixture was concentrated onto silica gel and purified by flash column chromatography (0–100% EtOAc in cyclohexane) to give the title compound (22 mg, 27%). HRMS (ESI) *m/z* calcd for C₂₁H₂₁N₄O₂ (M + H) 361.1659, found 361.1661. ¹H NMR (500 MHz, CDCl₃) δ 8.96 (s, 1H), 7.78–7.69 (m, 2H), 7.61 (d, *J* = 8.6 Hz, 1H), 7.54 (s, 1H), 7.47 (dd, *J* = 7.0, 1.0 Hz, 1H), 7.33–7.23 (m, 2H), 6.73 (s, 1H), 6.58–6.49 (m, 2H), 3.99 (s, 3H), 3.85 (s, 3H), 3.83 (s, 3H).

Preparation of Compounds in Scheme 2 (Exemplified by the Preparation of Compounds 24a, 24d, 28a, and 28b). **8-(1-Methyl-1H-pyrazol-4-yl)-2-(methylthio)pyrido[3,4-*d*]pyrimidine 17.** A solution of 8-chloro-2-(methylthio)pyrido[3,4-*d*]pyrimidine **16** (480 mg, 2.27 mmol), (1-methyl-1H-pyrazol-4-yl)boronic acid pinacol ester (940 mg, 4.52 mmol), and Pd(dppf)Cl₂·CH₂Cl₂ (100 mg, 0.122 mmol) in THF (15 mL) and sodium carbonate (2 M, 5 mL) was heated to 65 °C for 18 h. The mixture was diluted with EtOAc and quenched with brine. The aqueous layer was extracted with EtOAc three times. The combined organics were washed with water and brine, dried, and concentrated in vacuo. The residue was purified by flash column chromatography (0–4% MeOH in CH₂Cl₂) to give the title compound (658 mg, quant). HRMS (ESI) *m/z* calcd for C₁₂H₁₂N₅S (M + H) 258.0813, found 258.0817. ¹H NMR (500 MHz, CDCl₃) δ 9.22 (s, 1H), 8.67 (s, 1H), 8.63–8.56 (m, 2H), 7.47 (d, *J* = 5.3 Hz, 1H), 4.05 (s, 3H), 2.78 (s, 3H).

8-Cyclopropyl-2-(methylthio)pyrido[3,4-*d*]pyrimidine 18. A solution of 8-chloro-2-(methylthio)pyrido[3,4-*d*]pyrimidine **16** (20 mg, 0.094 mmol), cyclopropyl boronic acid (11 mg, 0.13 mmol), PCy₃ (3 mg, 11 μmol), K₃PO₄ (70 mg, 0.32 mmol), and Pd(OAc)₂ (1.0 mg, 4.5 μmol) was dissolved in toluene/water (6:1, 1 mL) and heated to 95 °C for 18 h. The mixture was diluted with EtOAc and quenched with brine. The aqueous layer was extracted with EtOAc three times. The combined organics were washed with water and brine, dried, and concentrated in vacuo. The residue was purified by flash column chromatography (0–20% EtOAc in cyclohexane) to give the title compound (13 mg, 62%). HRMS (ESI) *m/z* calcd for C₁₁H₁₂N₅S (M + H) 218.0746, found 218.0751. ¹H NMR (500 MHz, CDCl₃) δ 9.18 (s, 1H), 8.46 (d, *J* = 5.4 Hz, 1H), 7.37 (d, *J* = 5.5 Hz, 1H), 3.46 (tt, *J* = 8.2, 4.8 Hz, 1H), 2.74 (s, 3H), 1.34–1.27 (m, 2H), 1.25–1.17 (m, 2H).

8-(1-Methyl-1H-pyrazol-4-yl)-2-(methylsulfonyl)pyrido[3,4-*d*]pyrimidine 19. A suspension of 8-(1-methyl-1H-pyrazol-4-yl)-2-(methylthio)pyrido[3,4-*d*]pyrimidine **17** (584 mg, 2.27 mmol) in CH₂Cl₂ (22 mL) was treated with *m*-CPBA (77% w/w, 1.12 g, 4.98 mmol) at 0 °C and then allowed to reach rt over 18 h. The mixture was quenched with water and extracted with CH₂Cl₂. The combined organics were washed with water, dried, and concentrated in vacuo. The residue was purified by flash column chromatography (0–100% EtOAc in cyclohexane) to give the title compound (408 mg, 62%). HRMS (ESI) *m/z* calcd for C₁₂H₁₂N₅O₂S (M + H) 290.0706, found 290.0722. ¹H NMR (500 MHz, (CD₃)₂SO) δ 10.00 (s, 1H), 8.91 (d, *J* = 5.4 Hz, 1H), 8.81 (s, 1H), 8.53 (s, 1H), 7.99 (d, *J* = 5.4 Hz, 1H), 3.99 (s, 3H), 3.59 (s, 3H).

8-Cyclopropyl-2-(methylsulfonyl)pyrido[3,4-*d*]pyrimidine 20. A suspension of 8-cyclopropyl-2-(methylthio)pyrido[3,4-*d*]pyrimidine **18** (127 mg, 0.584 mmol) in CH₂Cl₂ (5 mL) was treated with *m*-CPBA (77% w/w, 290 mg, 1.29 mmol) at 0 °C and then allowed to reach rt over 18 h. The mixture was quenched with water and extracted with CH₂Cl₂. The combined organics were washed with water, dried, and concentrated onto silica. The residue was purified by flash column chromatography (0–70% EtOAc in cyclohexane) to give the title compound (128 mg, 88%). HRMS (ESI) *m/z* calcd for C₁₁H₁₂N₅O₂S (M + H) 250.0645, found 250.0648. ¹H NMR (500 MHz, (CD₃)₂SO) δ 9.99 (s, 1H), 8.79 (d, *J* = 5.5 Hz, 1H), 7.94 (d, *J* = 5.5 Hz, 1H), 3.56 (s, 3H), 3.44 (m, 1H), 1.30–1.25 (m, 2H), 1.24–1.20 (m, 2H).

***N*-(4-Methoxyphenyl)-8-(1-methyl-1H-pyrazol-4-yl)pyrido[3,4-*d*]pyrimidin-2-amine 24a.** To a solution of 8-(1-methyl-1H-pyrazol-4-yl)-2-(methylsulfonyl)pyrido[3,4-*d*]pyrimidine **19** (29 mg, 0.10 mmol) in DMSO (4 mL) was added cesium carbonate (59 mg, 0.18 mmol) and *N*-(4-methoxyphenyl)formamide (15 mg, 0.10 mmol). The mixture was heated to 100 °C for 18 h. The mixture was diluted with EtOAc and water. The aqueous layer was re-extracted with EtOAc. The combined organics were washed with brine, dried, and concentrated in vacuo. The residue was purified by flash column chromatography (0–10% MeOH in CH₂Cl₂), followed by SCX-2 cartridge (MeOH - 1 M NH₃ in MeOH) to give the title compound (8 mg, 24%). HRMS (ESI) *m/z* calcd for C₁₈H₁₆N₆O (M + H) 333.1464, found 333.1450. ¹H NMR (500 MHz, CD₃OD) δ 9.24 (s, 1H), 8.38 (s, 1H), 8.29 (d, *J* = 5.4 Hz, 1H), 7.63–7.59 (m, 3H), 7.54 (d, *J* = 5.4 Hz, 1H), 7.05 (d, *J* = 8.9 Hz, 2H), 3.91 (s, 3H), 3.87 (s, 3H).

8-Cyclopropyl-*N*-(2-methoxy-4-(1-methyl-1H-pyrazol-4-yl)phenyl)pyrido[3,4-*d*]pyrimidin-2-amine 24d. A solution of 2-methoxy-4-(1-methyl-1H-pyrazol-4-yl)aniline **23** (50 mg, 0.25 mmol), TFA (45 μL, 0.60 mmol), and 8-cyclopropyl-2-(methylsulfonyl)pyrido[3,4-*d*]pyrimidine **20** (31 mg, 0.12 mmol) in 2,2,2-trifluoroethanol (0.7 mL) was heated to 130 °C under microwave irradiation for 1.5 h. The reaction was diluted with EtOAc and quenched with aqueous sat. sodium bicarbonate. The aqueous layer was extracted with EtOAc, and the combined organics were washed with water and brine, dried, and concentrated in vacuo. The residue was purified by flash column chromatography (0–60% EtOAc in cyclohexane) to give the title compound (20 mg, 43%). HRMS (ESI) *m/z* calcd for C₂₁H₂₁N₆O (M + H) 373.1771, found 373.1773. ¹H NMR (500 MHz, (CD₃)₂SO) δ 9.40 (s, 1H), 8.54 (s, 1H), 8.41 (d, *J* = 8.3 Hz, 1H), 8.28 (d, *J* = 5.3 Hz, 1H), 8.17 (d, *J* = 0.9 Hz, 1H), 7.90 (d, *J* = 0.8 Hz, 1H), 7.56 (d, *J* = 5.3 Hz, 1H), 7.30 (d, *J* = 1.8 Hz, 1H), 7.25 (dd, *J* = 8.2, 1.8 Hz, 1H), 3.96 (s, 3H), 3.88 (s, 3H), 3.24 (m, 1H), 1.16–1.08 (m, 4H).

Preparation of Formamides 26b–e (Exemplified by Preparation of Compound 26b). ***N*-(2-Methyl-4-(1-methyl-1H-pyrazol-4-yl)phenyl)formamide 26b.** A solution of 2-methyl-4-(1-methyl-1H-pyrazol-4-yl)aniline **S1** (100 mg, 0.534 mmol) in formic acid (3 mL) was heated to 100 °C for 3 h. The mixture was concentrated in vacuo. The residue was partitioned between aqueous sat. sodium bicarbonate and EtOAc. The aqueous layer was re-extracted with EtOAc. The combined organics were washed with water and brine, dried, and concentrated in vacuo. The residue was purified by flash column chromatography (0–10% MeOH in EtOAc) to give the title compound (160 mg, 34%). HRMS (ESI) *m/z* calcd for C₁₂H₁₄N₃O (M + H) 216.1131, found 216.1141. ¹H NMR (500 MHz, CD₃OD) δ 8.31 (s, 1H), 7.93 (s, 1H), 7.80 (s, 1H), 7.67 (d, *J* = 8.0 Hz, 1H), 7.44 (d, *J* = 2.0 Hz, 1H), 7.38 (dd, *J* = 8.0, 2.0 Hz, 1H), 3.92 (s, 3H), 2.31 (s, 3H).

8-Chloro-*N*-(2-methyl-4-(1-methyl-1H-pyrazol-4-yl)phenyl)pyrido[3,4-*d*]pyrimidin-2-amine 27b. To a cooled (0 °C) suspension of *N*-(2-methyl-4-(1-methyl-1H-pyrazol-4-yl)phenyl)formamide **26b** (40 mg, 0.19 mmol) in THF (4 mL) was added sodium hydride (60% w/w dispersion in oil, 12 mg, 0.30 mmol). The reaction mixture was stirred at rt for 10 min. The mixture was cooled to 0 °C, and 8-chloro-2-(methylthio)pyrido[3,4-*d*]pyrimidine **25**¹⁶ (60 mg, 0.24 mmol) was added. The mixture was stirred for 18 h while slowly warming to rt and then concentrated in vacuo, and the residue was partitioned between EtOAc and water. The aqueous layer was extracted with EtOAc and CH₂Cl₂. The combined organics were washed with water and brine, dried, and concentrated in vacuo. The residue was purified by flash column chromatography (0–5% MeOH in EtOAc) to give the title compound (79 mg, 97%). HRMS (ESI) *m/z* calcd for C₁₉H₁₆ClN₆ (M + H) 351.1119, found 351.1111. ¹H NMR (500 MHz, CDCl₃) δ 9.17 (s, 1H), 8.26 (d, *J* = 5.0 Hz, 1H), 7.79 (s, 1H), 7.63 (s, 1H), 7.52 (d, *J* = 5.0 Hz, 1H), 7.47 (dd, *J* = 8.0, 2.0 Hz, 1H), 7.42 (m, 1H), 7.39 (d, *J* = 2.0 Hz, 1H), 3.98 (s, 3H), 2.44 (s, 3H).

***N*-(2-Methoxy-4-(1-methyl-1H-pyrazol-4-yl)phenyl)-8-phenylpyrido[3,4-*d*]pyrimidin-2-amine 28a.** To a solution of 8-chloro-*N*-(2-methoxy-4-(1-methyl-1H-pyrazol-4-yl)phenyl)pyrido[3,4-*d*]pyrimidin-2-amine **27a**¹⁶ (25 mg, 0.068 mmol) in 1,4-dioxane/water (2:1, 3 mL) was added phenyl boronic acid (17 mg, 0.14 mmol), Pd(PPh₃)₄ (16 mg, 0.014 mmol), and cesium carbonate (33 mg, 0.10

mmol). The reaction was heated to 100 °C under microwave irradiation for 30 min. The reaction was diluted with EtOAc and water, dried, and concentrated in vacuo. The residue was purified by flash column chromatography (0–100% EtOAc in cyclohexane) followed by SCX-2 cartridge (MeOH - 1 M NH₃ in MeOH) to give the title compound (8 mg, 29%). HRMS (ESI) *m/z* calcd for C₂₄H₂₁N₆O (M + H) 409.1777, found 409.1771. ¹H NMR (500 MHz, CD₃OD) δ 9.37 (s, 1H), 8.56 (d, *J* = 8.5 Hz, 1H), 8.50 (d, *J* = 5.5 Hz, 1H), 8.11–8.09 (m, 2H), 7.97 (s, 1H), 7.82 (s, 1H), 7.79 (d, *J* = 5.5 Hz, 1H), 7.61–7.59 (m, 3H), 7.19 (d, *J* = 2.0 Hz, 1H), 6.99 (dd, *J* = 8.5, 2.0 Hz, 1H), 4.02 (s, 3H), 3.95 (s, 3H).

8-(1-Methyl-1H-pyrazol-4-yl)-N-(2-methyl-4-(1-methyl-1H-pyrazol-4-yl)phenyl)pyrido[3,4-d]pyrimidin-2-amine 28b. To a solution of 8-chloro-N-(2-methyl-4-(1-methyl-1H-pyrazol-4-yl)phenyl)pyrido[3,4-d]pyrimidin-2-amine **27b** (12 mg, 0.034 mmol) in 1,4-dioxane/water (2:1, 3 mL) were added 1-methyl-4-(4,4,5,5-tetramethyl-1,3,2-dioxaborolan-2-yl)-1H-pyrazole (14 mg, 0.068 mmol), cesium carbonate (17 mg, 0.051 mmol), and Pd(PPh₃)₄ (2 mg, 1.7 μmol). The reaction mixture was heated to 100 °C under microwave conditions for 30 min. The reaction mixture was diluted with EtOAc and water. The combined organics were washed with water and brine, dried, and concentrated in vacuo. The residue was purified by flash column chromatography (0–15% MeOH in EtOAc) to give the title compound (7 mg, 52%). HRMS (ESI) *m/z* calcd for C₂₂H₂₁N₈ (M + H) 397.1884, found 397.1878. ¹H NMR (500 MHz, CDCl₃) δ 9.16 (s, 1H), 8.43 (d, *J* = 5.5 Hz, 1H), 8.40 (d, *J* = 5.5 Hz, 2H), 7.86 (d, *J* = 8.0 Hz, 1H), 7.82 (s, 1H), 7.67 (s, 1H), 7.50–7.45 (m, 2H), 7.36 (d, *J* = 5.5 Hz, 1H), 7.05 (br s, 1H), 4.00 (s, 3H), 3.77 (s, 3H), 2.39 (s, 3H).

Preparation of Compounds in Scheme 3 (Exemplified by the Preparation of 33a). **2-(Methylsulfonyl)-8-(pyrrolidin-1-yl)pyrido[3,4-d]pyrimidine 31.** A mixture of 8-chloro-2-(methylthio)pyrido[3,4-d]pyrimidine **16** (105 mg, 0.496 mmol) and pyrrolidine (425 μL, 5.10 mmol) in NMP (2.5 mL) was stirred at 135 °C for 3 h. The mixture was quenched with aqueous sat. sodium bicarbonate and extracted with EtOAc. The combined organics were washed with water and brine, dried, and concentrated in vacuo to afford the crude sulfide.

A suspension of crude sulfide **29** (ca. 0.496 mmol) in CH₂Cl₂ (4 mL) was treated with *m*-CPBA (77% w/w, 250 mg, 1.11 mmol) at 0 °C and then allowed to reach rt for 18 h. An additional portion of *m*-CPBA (77% w/w, 60 mg, 0.27 mmol) was added at rt, and the mixture stirred for 2 h. The mixture was quenched with water and extracted with CH₂Cl₂. The combined organics were washed with aqueous sat. sodium bicarbonate and brine, dried, and concentrated in vacuo. The residue was purified by flash column chromatography (0–70% EtOAc in cyclohexane) to give the title compound (62 mg, 45% over two steps). LCMS (ESI) *m/z* 279 (M + H). ¹H NMR (500 MHz, (CD₃)₂SO) δ 9.62 (s, 1H), 8.30 (d, *J* = 5.4 Hz, 1H), 7.11 (d, *J* = 5.5 Hz, 1H), 3.97 (br s, 4H), 3.45 (s, 3H), 1.98 (s, 4H).

N-(2-Methoxy-4-(1-methyl-1H-pyrazol-4-yl)phenyl)-8-(pyrrolidin-1-yl)pyrido[3,4-d]pyrimidin-2-amine 33a. A solution of 2-methoxy-4-(1-methyl-1H-pyrazol-4-yl)aniline **23** (52 mg, 0.26 mmol), TFA (50 μL, 0.65 mmol) and 2-(methylsulfonyl)-8-(pyrrolidin-1-yl)pyrido[3,4-d]pyrimidine **31** (35 mg, 0.13 mmol) in 2,2,2-trifluoroethanol (0.6 mL) was heated to 130 °C under microwave irradiation for 2 h. An additional portion of TFA (50 μL, 0.65 mmol) was added, and the mixture was heated to 180 °C under microwave irradiation for 2 h. The reaction mixture was diluted with EtOAc, quenched with aqueous sat. sodium bicarbonate, and the aqueous layer extracted with EtOAc. The combined organics were washed with water and brine, dried, concentrated in vacuo, and purified by flash column chromatography (0–100% EtOAc in cyclohexane) to give the title compound (10 mg, 20%). HRMS (ESI) *m/z* calcd for C₂₂H₂₄N₇O (M + H) 402.2037, found 402.2040. ¹H NMR (500 MHz, (CD₃)₂SO) δ 9.12 (s, 1H), 8.37 (s, 1H), 8.14 (s, 1H), 7.88 (d, *J* = 0.9 Hz, 1H), 7.87–7.79 (m, 2H), 7.24 (d, *J* = 1.9 Hz, 1H), 7.17 (dd, *J* = 8.2, 1.9 Hz, 1H), 6.86 (d, *J* = 5.4 Hz, 1H), 3.89 (s, 3H), 3.87 (s, 3H), 3.84–3.76 (m, 4H), 1.91–1.81 (m, 4H).

Preparation of Compounds in Scheme 4 (Exemplified by the Preparation of Compounds 34a, 34f, and 38). **N⁸-Isobutyl-N²-(2-methoxy-4-(1-methyl-1H-pyrazol-4-yl)phenyl)pyrido[3,4-d]pyrimidine-2,8-diamine 34a.** A mixture of 8-chloro-N-(2-methoxy-4-(1-methyl-1H-pyrazol-4-yl)phenyl)pyrido[3,4-d]pyrimidin-2-amine

27a¹⁶ (27 mg, 0.074 mmol) and 2-methylpropan-1-amine (100 μL, 1.0 mmol) in NMP (0.7 mL) was stirred at 130 °C in a closed cap vial for 5 h. The reaction mixture was quenched with aqueous sat. sodium bicarbonate and extracted with EtOAc. The combined organics were washed with water and brine, dried, and concentrated in vacuo. The residue was purified by flash column chromatography (0–80% EtOAc in cyclohexane) to give the title compound (19 mg, 63%). HRMS (ESI) *m/z* calcd for C₂₂H₂₆N₇O (M + H) 404.2193, found 404.2177. ¹H NMR (500 MHz, (CD₃)₂SO) δ 9.16 (s, 1H), 8.43 (s, 1H), 8.19 (d, *J* = 8.3 Hz, 1H), 8.15 (d, *J* = 0.8 Hz, 1H), 7.88 (d, *J* = 0.8 Hz, 1H), 7.77 (d, *J* = 5.7 Hz, 1H), 7.27 (d, *J* = 1.9 Hz, 1H), 7.18 (dd, *J* = 8.2, 1.9 Hz, 1H), 6.88–6.85 (m, 2H), 3.93 (s, 3H), 3.87 (s, 3H), 3.39–3.28 (m, 2H), 2.00 (hept, *J* = 6.8 Hz, 1H), 0.95 (d, *J* = 6.7 Hz, 6H).

8-(Cyclohexylthio)-N-(2-methoxy-4-(1-methyl-1H-pyrazol-4-yl)phenyl)pyrido[3,4-d]pyrimidin-2-amine 34f. A mixture of 8-chloro-N-(2-methoxy-4-(1-methyl-1H-pyrazol-4-yl)phenyl)pyrido[3,4-d]pyrimidin-2-amine **27a**¹⁶ (26 mg, 0.071 mmol) and potassium carbonate (15 mg, 0.11 mmol) in DMF (0.35 mL) was treated with cyclohexanethiol (12 μL, 0.098 mmol) and stirred at rt for 4 d. An additional batch of potassium carbonate (10 mg, 0.070 mmol) and cyclohexanethiol (12 μL, 0.098 mmol) was added, and the mixture stirred at 50 °C for 18 h. The reaction was quenched with brine and extracted with EtOAc. The combined organics were washed with water and brine, dried, and concentrated in vacuo. The residue was purified by flash column chromatography (0–80% EtOAc in cyclohexane) to give the title compound (30 mg, 94%). HRMS (ESI) *m/z* calcd for C₂₄H₂₇N₆OS (M + H) 447.1962, found 447.1948. ¹H NMR (500 MHz, (CD₃)₂SO) δ 9.35 (s, 1H), 8.55 (br s, 1H), 8.29 (d, *J* = 5.4 Hz, 1H), 8.20 (d, *J* = 0.9 Hz, 1H), 7.93 (d, *J* = 0.8 Hz, 1H), 7.48 (d, *J* = 5.4 Hz, 1H), 7.29 (d, *J* = 1.9 Hz, 1H), 7.26 (dd, *J* = 8.2, 1.9 Hz, 1H), 3.96 (br s, 4H), 3.87 (s, 3H), 2.17–2.05 (m, 2H), 1.82–1.72 (m, 2H), 1.65 (m, 1H), 1.59–1.40 (m, 4H), 1.35 (m, 1H).

8-(Cyclopropylmethoxy)-2-(methylthio)pyrido[3,4-d]pyrimidine 36. A suspension of 2-(methylthio)pyrido[3,4-d]pyrimidin-8(7H)-one **35**¹⁶ (502 mg, 2.60 mmol) and silver carbonate (988 mg, 3.58 mmol) in CHCl₃ (25 mL) was treated with bromomethyl cyclopropane (310 μL, 3.19 mmol) and stirred at rt for 18 h. The mixture was heated to 60 °C for 4 h, and an additional batch of bromomethyl cyclopropane (310 μL, 3.19 mmol) was added. The reaction was heated to 60 °C for 18 h. An additional batch of bromomethyl cyclopropane (310 μL, 3.19 mmol) was added and heated for a further 2 h. Et₃N was added (6 mL), the mixture filtered through Celite (CH₂Cl₂), and concentrated in vacuo. The residue was purified by flash column chromatography (0–80% EtOAc in cyclohexane) to give the title compound (112 mg, 17%). LCMS (ESI) *m/z* 248 (M + H). ¹H NMR (500 MHz, CDCl₃) δ 9.14 (s, 1H), 8.07 (d, *J* = 5.6 Hz, 1H), 7.18 (d, *J* = 5.6 Hz, 1H), 4.43 (d, *J* = 7.0 Hz, 2H), 2.74 (s, 3H), 1.48 (m, 1H), 0.73–0.61 (m, 2H), 0.54–0.43 (m, 2H).

8-(Cyclopropylmethoxy)-2-(methylsulfonyl)pyrido[3,4-d]pyrimidine 37. A suspension of 8-(cyclopropylmethoxy)-2-(methylthio)pyrido[3,4-d]pyrimidine **31** (110 mg, 0.445 mmol) in CH₂Cl₂ (4 mL) was treated with *m*-CPBA (77% w/w, 325 mg, 1.35 mmol) at 0 °C and then allowed to reach rt for 18 h. The mixture was quenched with water and extracted with CH₂Cl₂. The combined organics were washed with aqueous sat. sodium bicarbonate, dried, and concentrated in vacuo. The residue was purified by flash column chromatography (0–55% EtOAc in cyclohexane) to give the title compound (95 mg, 77%). HRMS (ESI) *m/z* calcd C₁₂H₁₄N₃O₃S (M + H) 280.0750, found 280.0748. ¹H NMR (500 MHz, (CD₃)₂SO) δ 9.92 (s, 1H), 8.44 (d, *J* = 5.7 Hz, 1H), 7.72 (d, *J* = 5.7 Hz, 1H), 4.43 (d, *J* = 7.2 Hz, 2H), 3.50 (s, 3H), 1.41 (m, 1H), 0.69–0.57 (m, 2H), 0.49–0.40 (m, 2H).

8-(Cyclopropylmethoxy)-N-(2-methoxy-4-(1-methyl-1H-pyrazol-4-yl)phenyl)pyrido[3,4-d]pyrimidin-2-amine 38. A solution of N-(2-methoxy-4-(1-methyl-1H-pyrazol-4-yl)phenyl)formamide **26a** (30 mg, 0.13 mmol) in THF (1 mL) was treated with sodium hydride (60% w/w dispersion in oil, 8 mg, 0.20 mmol) at 0 °C. After stirring for 40 min at rt, the mixture was cooled to 0 °C, and 8-(cyclopropylmethoxy)-2-(methylsulfonyl)pyrido[3,4-d]pyrimidine **37** (46 mg, 0.17 mmol) was added. The reaction was allowed to reach rt and stirred for 18 h. Sodium

hydroxide (2 M, 1 mL) and MeOH (1 mL) were added, and the resulting mixture stirred at rt for 3 h. The mixture was concentrated in vacuo. The residue was partitioned between EtOAc and water. The aqueous layer was extracted with EtOAc, and the combined organics were washed with water and brine, dried, and concentrated in vacuo. The residue was purified by flash column chromatography (0–75% EtOAc in cyclohexane) to give the title compound (27 mg, 52%). HRMS (ESI) m/z calcd for $C_{22}H_{23}N_6O_2$ (M + H) 403.1877, found 403.1871. 1H NMR (500 MHz, $(CD_3)_2SO$) δ 9.31 (s, 1H), 8.61 (s, 1H), 8.39 (s, 1H), 8.17 (d, $J = 0.8$ Hz, 1H), 7.94–7.84 (m, 2H), 7.35 (d, $J = 5.6$ Hz, 1H), 7.28 (d, $J = 1.8$ Hz, 1H), 7.19 (dd, $J = 8.3, 1.8$ Hz, 1H), 4.33 (d, $J = 6.9$ Hz, 2H), 3.94 (s, 3H), 3.88 (s, 3H), 1.40 (m, 1H), 0.68–0.59 (m, 2H), 0.49–0.39 (m, 2H).

Biochemical Assays. MPS1, CDK2, and Aurora A and B counterscreen assays were performed as reported previously.⁷

MSD Assay. IC₅₀ of MPS1 autophosphorylation inhibition at pTpS^{33/37} sites in HCT116 cells was determined by an electrochemiluminescence assay (Meso Scale Discovery, MSD) as described previously.⁷

Cell Viability Assay. Cell proliferation assays were carried out by colorimetric 3-(4,5-dimethylthiazol-2-yl)-2,5-diphenyltetrazolium bromide (MTT) assay (Sigma) in HCT116 cells as described previously.⁷

Crystallization. The kinase domain (residues 519–808) of MPS1 was produced in *E. coli* and purified as described previously.^{10c} For compound **39**, apo crystals of MPS1 were grown in PEG300 as previously described⁷ prior to soaking in a fresh solution containing 35% PEG300, 1 mM inhibitor, and 1% (v/v) DMSO for 24 h. The crystal was cryo-protected in soak solution supplemented with 22.5% ethylene glycol prior to flash cooling in liquid nitrogen.

Co-crystals of MPS1 with compound **S11** were grown at 18 °C using the sitting-drop vapor-diffusion method. The crystallization drops were composed of 2 μ L of protein/ligand solution (8.9 mg/mL protein and 5 mM **S11**) and 2 μ L of reservoir solution placed over 200 μ L of reservoir solution of 18–26% (w/v) PEG3350, 0.1 M bis-Tris propane pH 7.5, 0.1 M MgCl₂, and 0.1 M sodium formate in 48-well plates. Co-crystals typically grew in 12–16 h. Crystals of MPS1 with **S11** were transferred to backsoaking solutions containing reservoir solution also containing 200 mM of inhibitor and up to 20% (v/v) DMSO and incubated at 18 °C for 24–48 h. Crystals were cryo-protected with paratone-N oil prior to flash cooling in liquid nitrogen.

Co-crystals of MPS1 with compound **34e** were grown at 18 °C using the sitting-drop vapor-diffusion method. The crystallization drops were composed of 2 μ L of protein/ligand solution (11.4 mg/mL protein and 2 mM **34e**) with 20% (w/v) PEG3350, 0.1 M bis-Tris propane pH 7.5, and 0.2 M sodium formate. Crystals were cryo-protected with paratone-N oil prior to flash cooling in liquid nitrogen.

Data Collection, Structure Solution, and Refinement. X-ray diffraction data were collected at 100 K at Diamond Light Source (Oxfordshire, U.K.) or in-house on a Rigaku FRX with Pilatus 300 K detector. Data were integrated with XDS²⁴ or MOSFLM (**S11** data set only).²⁵ All data were imported to MTZ format with POINTLESS,²⁶ then scaled and merged with AIMLESS²⁶ in the CCP4 suite.²⁵ The structures were solved by molecular replacement with PHASER,²⁷ with the PDB structure 4C4J⁷ as the search model after removal of all nonprotein atoms. Structures were refined in iterative cycles of model building with COOT²⁸ and refinement with BUSTER.²⁹ TLS groups were selected with PHENIX phenix.find_tls_groups.³⁰ Ligand restraints were generated with GRADE³¹ and MOGUL.³² The final structure quality was checked with MOLPROBITY.³³ The data collection and refinement statistics are presented in Table S7.

Microsomal Metabolism. Microsomal turnover was carried out in male CD1 mice, female Sprague–Dawley rats, and pooled human liver microsomes obtained from Tebu-Bio (Peterborough, U.K.) following 30 min incubation of 10 μ M compound in 1 mg/mL microsomal protein, 3 mmol/L MgCl₂, 1 mmol/L NADPH, 2.5 mmol/L UDP-glucuronic acid, and 10 mmol/L phosphate buffer (pH 7.4) (all purchased from Sigma-Aldrich, Gillingham, U.K.). Reactions, at 37 °C, were started by addition of the test compound and were terminated at 0 and 30 min by the addition of 3 volumes of ice-cold methanol containing internal standard. Samples were centrifuged at 2800g for 30 min at 4 °C

and the supernatants analyzed. Control incubations were prepared as above with omission of cofactors. Compound measurements were performed by LCMS on an Agilent quadrupole time-of-flight instrument (Agilent 6510) following separation with a 6 min gradient of 10 mM ammonium acetate in methanol on a 50 \times 2.1 mm 2.6 μ m particles C18 column (Kinetex Phenomenex). For metabolite identification, the gradient was extended to 20 min, and MS/MS carried out with fragment elucidation for ions of interest.

Pharmacokinetic Studies. All in vivo studies were performed in accordance with U.K. Home Office regulations, ICR ethical review processes, and U.K. National Cancer Research Institute guidelines.³⁴ Female Balb/C mice and Sprague–Dawley rats were obtained from Charles River (Margate, U.K.). Animals were adapted to laboratory conditions for at least 1 week prior to dosing and were allowed food and water ad libitum. Compounds were administered iv or po (mouse: 0.1 mL/10g in 10% DMSO, 5% tween 20 in saline, rat: 0.05 mL/10g in 10% DMSO, 5% tween 20 in saline). Blood samples were collected from the tail vein (20 μ L) at 8 time points over the 24 h post dose and spotted on Whatman B cards together with a standard curve and quality controls spiked in control blood. Cards were allowed to dry at rt for at least 6 h. Cards were punched, and 6 mm discs were extracted with 200 μ L methanol containing 500 nM olomoucine as an internal standard. Following centrifugation, extracts were analyzed by multiple reaction monitoring of precursor and product ions by ESI-LCMS/MS on a QTRAP 4000 (ABSciex) following separation as above. Quantitation was carried out with an external calibration (8 points ranging from 1 nM to 25 μ M). Quality controls were included (3 concentrations) at the beginning and the end of the analytical run and were within 20% of nominal concentrations.

Pharmacokinetic parameters were derived from noncompartmental analysis WiniNONlin (model 200 and 201) Pharsight version.

In Vivo Proof-of-Concept Studies. Animals (6–8 week old female NCr athymic mice) were supplied by a commercial breeder and fed sterilized food and water ad libitum.

PK/PD Study. Three million HCT116 human colorectal carcinoma cells were injected s.c. bilaterally into the flanks. Dosing commenced when tumors reached a mean diameter of 8–10 mm (day 14). Animals ($n = 6$ per group) were dosed twice daily with compound **34h** (100 mg/kg po) or vehicle (10% DMSO, 5% Tween 20, 85% saline) over 3 days (6 doses), and groups of three were culled at 2 or 6 h after the final dose. Heparinized plasma and tumor samples were collected and snap frozen for pharmacokinetic (PK) and pharmacodynamic (PD) biomarker analysis.

PD Assays. For PD analysis, frozen tumor samples were homogenized in RIPA lysis buffer (150 mM NaCl, 50 mM Tris pH 7.5, 1 mM EDTA pH 8.0, 1% NP40, 1% sodium deoxycholate, 1% sodium dodecyl sulfate, and supplemented with protease and phosphatase inhibitors), sonicated, and centrifuged to clear the debris. Protein concentrations of the supernatants were measured, and 5 μ g protein for each sample was loaded onto LDS-PAGE (Life technologies). Proteins were separated, transferred to nitrocellulose membrane, and probed with phospho-histone H3 (Millipore), total-histone H3 (Abcam), cleaved-PARP (Cell Signaling), and GAPDH (Millipore) antibodies. Blots were quantified using ImageJ and analyzed with Graphpad Prism.

■ ASSOCIATED CONTENT

📄 Supporting Information

The Supporting Information is available free of charge on the ACS Publications website at DOI: 10.1021/acs.jmedchem.5b01811.

Additional data (CSV)

Experimental procedures and analytical data for final compounds **24b**, **24c**, **28c**, **28d**, **28e**, **33b**, **34b–e**, **34g**, **34h**, intermediates and formamides. Aurora A and B inhibition data available for all compounds. CYP and hERG activity as well as kinase selectivity profiling of **34h**.

Crystallographic analysis of compounds **15b**, **24b**, **24c**, **34e**, **39** bound to MPS1 (PDF)

Accession Codes

Atomic coordinates and structure factors for compounds **1**, **15b**, **24b**, **24c**, **34e** and **39** can be accessed using PDB codes 4C4J, SEI6, SEI2, SEI8, SEH0, SEHY, respectively.

AUTHOR INFORMATION

Corresponding Author

*E-mail: swen.hoelder@icr.ac.uk. Phone: +44 (0)2087224353.

Present Address

^{||}SBA School of Science and Engineering, Lahore University of Management Sciences, D.H.A., Lahore 54792, Pakistan.

Notes

The authors declare no competing financial interest.

ACKNOWLEDGMENTS

This work was supported by Cancer Research U.K. [grant number C309/A11566]. We also acknowledge the Cancer Research Technology Pioneer Fund and Sixth Element Capital for funding (to P.I.) and NHS funding to the NIHR Biomedical Research Centre. S.L. is also supported by Breakthrough Breast Cancer (recently merged with Breast Cancer Campaign forming Breast Cancer Now). We thank the staff of DIAMOND Light Source for their support during data collection. We thank Dr. Amin Mirza, Dr. Maggie Liu, and Mr. Meirion Richards for their help with LC, NMR, and mass spectrometry.

ABBREVIATIONS USED

CDK2, cyclin-dependent kinase 2; Cl, clearance; hERG, human ether-à-go-go-related gene; HLM, human liver microsomes; JNK1, c-Jun N-terminal kinase 1; JNK2, c-Jun N-terminal kinase 2; L.E., ligand efficiency; L.L.E, lipophilic ligand efficiency; LRRK, leucine-rich repeat kinase; MLM, mouse liver microsomes; MPS1, monopolar spindle kinase 1; MSD, Meso Scale Discovery; MTT, 3-(4,5-dimethylthiazol-2-yl)-2,5-diphenyltetrazolium bromide; PARP, poly ADP ribose polymerase; PLK1, polo-like kinase 1; PTEN, phosphatase and tensin homologue; SAC, spindle assembly checkpoint; RLM, rat liver microsomes; TGI, tumor growth inhibition; V_{ss} , volume of distribution

REFERENCES

(1) (a) Jackson, J. R.; Patrick, D. R.; Dar, M. M.; Huang, P. S. Targeted anti-mitotic therapies: can we improve on tubulin agents? *Nat. Rev. Cancer* **2007**, *7*, 107–117. (b) Wood, K. W.; Cornwell, W. D.; Jackson, J. R. Past and future of the mitotic spindle as an oncology target. *Curr. Opin. Pharmacol.* **2001**, *1*, 370–377. (c) Chan, K. S.; Koh, C. G.; Li, H. Y. Mitosis-targeted anti-cancer therapies: where they stand. *Cell Death Dis.* **2012**, *3*, e411.

(2) (a) Hardwick, K. G. The spindle checkpoint. *Trends Genet.* **1998**, *14*, 1–4. (b) Mills, G. B.; Schmandt, R.; McGill, M.; Amendola, A.; Hill, M.; Jacobs, K.; May, C.; Rodricks, A. M.; Campbell, S.; Hogg, D. Expression of TTK, a novel human protein kinase, is associated with cell proliferation. *J. Biol. Chem.* **1992**, *267*, 16000–16006. (c) Lauze, E.; Stoelcker, B.; Luca, F. C.; Weiss, E.; Schutz, A. R.; Winey, M. Yeast spindle pole body duplication gene MPS1 encodes an essential dual specificity protein kinase. *EMBO J.* **1995**, *14*, 1655–1663. (d) Musacchio, A.; Salmon, E. D. The spindle-assembly checkpoint in space and time. *Nat. Rev. Mol. Cell Biol.* **2007**, *8*, 379–393.

(3) (a) Daniel, J.; Coulter, J.; Woo, J.-H.; Wilsbach, K.; Gabrielson, E. High levels of the Mps1 checkpoint protein are protective of aneuploidy in breast cancer cells. *Proc. Natl. Acad. Sci. U. S. A.* **2011**, *108*, 5384–

5389. (b) Brough, R.; Frankum, J. R.; Sims, D.; MacKay, A.; Mendes-Pereira, A. M.; Bajrami, I.; Costa-Cabral, S.; Rafiq, R.; Ahmad, A. S.; Cerone, M. A.; Natrajan, R.; Sharpe, R.; Shiu, K.-K.; Wetterskog, D.; Dedes, K. J.; Lambros, M. B.; Rawjee, T.; Linardopoulos, S.; Reis-Filho, J. S.; Turner, N. C.; Lord, C. J.; Ashworth, A. Functional Viability Profiles of Breast Cancer. *Cancer Discovery* **2011**, *1*, 260–273. (c) Gordon, D. J.; Resio, B.; Pellman, D. Causes and consequences of aneuploidy in cancer. *Nat. Rev. Genet.* **2012**, *13*, 189–203.

(4) (a) Yuan, B.; Xu, Y.; Woo, J.-H.; Wang, Y.; Bae, Y. K.; Yoon, D.-S.; Wersto, R. P.; Tully, E.; Wilsbach, K.; Gabrielson, E. Increased Expression of Mitotic Checkpoint Genes in Breast Cancer Cells with Chromosomal Instability. *Clin. Cancer Res.* **2006**, *12*, 405–410. (b) Mizukami, Y.; Kono, K.; Daigo, Y.; Takano, A.; Tsunoda, T.; Kawaguchi, Y.; Nakamura, Y.; Fujii, H. Detection of novel cancer-testis antigen-specific T-cell responses in TIL, regional lymph nodes, and PBL in patients with esophageal squamous cell carcinoma. *Cancer Sci.* **2008**, *99*, 1448–1454. (c) Salvatore, G.; Nappi, T. C.; Salerno, P.; Jiang, Y.; Garbi, C.; Ugolini, C.; Miccoli, P.; Basolo, F.; Castellone, M. D.; Cirafici, A. M.; Melillo, R. M.; Fusco, A.; Bittner, M. L.; Santoro, M. A Cell Proliferation and Chromosomal Instability Signature in Anaplastic Thyroid Carcinoma. *Cancer Res.* **2007**, *67*, 10148–10158. (d) Thykjaer, T.; Workman, C.; Kruhoffer, M.; Demtroder, K.; Wolf, H.; Andersen, L. D.; Frederiksen, C. M.; Knudsen, S.; Orntoft, T. F. Identification of gene expression patterns in superficial and invasive human bladder cancer. *Cancer Res.* **2001**, *61*, 2492–2499.

(5) (a) Tannous, B. A.; Kerami, M.; Van der Stoop, P. M.; Kwiatkowski, N.; Wang, J.; Zhou, W.; Kessler, A. F.; Lewandrowski, G.; Hiddingh, L.; Sol, N.; Lagerweij, T.; Wedekind, L.; Niers, J. M.; Barazas, M.; Nilsson, R. J. A.; Geerts, D.; De Witt Hamer, P. C.; Hagemann, C.; Vandertop, W. P.; Van Tellingen, O.; Noske, D. P.; Gray, N. S.; Würdinger, T. Effects of the Selective MPS1 Inhibitor MPS1-IN-3 on Glioblastoma Sensitivity to Antimitotic Drugs. *J. Nat. Canc. Inst.* **2013**, *105*, 1322–1331. (b) Slee, R. B.; Grimes, B. R.; Bansal, R.; Gore, J.; Blackburn, C.; Brown, L.; Gasaway, R.; Jeong, J.; Victorino, J.; March, K. L.; Colombo, R.; Herbert, B. S.; Korc, M. Selective inhibition of pancreatic ductal adenocarcinoma cell growth by the mitotic MPS1 kinase inhibitor NMS-P715. *Mol. Cancer Ther.* **2014**, *13*, 307–315.

(6) Aarts, M.; Linardopoulos, S.; Turner, N. C. Tumour selective targeting of cell cycle kinases for cancer treatment. *Curr. Opin. Pharmacol.* **2013**, *13*, 529–535.

(7) Naud, S.; Westwood, I. M.; Faisal, A.; Sheldrake, P.; Bavetsias, V.; Atrash, B.; Cheung, K.-M. J.; Liu, M.; Hayes, A.; Schmitt, J.; Wood, A.; Choi, V.; Boxall, K.; Mak, G.; Gurden, M.; Valenti, M.; de Haven Brandon, A.; Henley, A.; Baker, R.; McAndrew, C.; Matijssen, B.; Burke, R.; Hoelder, S.; Eccles, S. A.; Raynaud, F. I.; Linardopoulos, S.; van Montfort, R. L. M.; Blagg, J. Structure-Based Design of Orally Bioavailable 1H-Pyrrolo[3,2-c]pyridine Inhibitors of Mitotic Kinase Monopolar Spindle 1 (MPS1). *J. Med. Chem.* **2013**, *56*, 10045–10065.

(8) (a) Kusakabe, K.-i.; Ide, N.; Daigo, Y.; Itoh, T.; Yamamoto, T.; Hashizume, H.; Nozu, K.; Yoshida, H.; Tadano, G.; Tagashira, S.; Higashino, K.; Okano, Y.; Sato, Y.; Inoue, M.; Iguchi, M.; Kanazawa, T.; Ishioka, Y.; Dohi, K.; Kido, Y.; Sakamoto, S.; Ando, S.; Maeda, M.; Higaki, M.; Baba, Y.; Nakamura, Y. Discovery of Imidazo[1,2-b]pyridazine Derivatives: Selective and Orally Available Mps1 (TTK) Kinase Inhibitors Exhibiting Remarkable Antiproliferative Activity. *J. Med. Chem.* **2015**, *58*, 1760–1775. (b) Laufer, R.; Ng, G.; Liu, Y.; Patel, N. K. B.; Edwards, L. G.; Lang, Y.; Li, S.-W.; Feher, M.; Awrey, D. E.; Leung, G.; Beletskaya, I.; Plotnikova, O.; Mason, J. M.; Hodgson, R.; Wei, X.; Mao, G.; Luo, X.; Huang, P.; Green, E.; Kiarash, R.; Lin, D. C.-C.; Harris-Brandts, M.; Ban, F.; Nadeem, V.; Mak, T. W.; Pan, G. J.; Qiu, W.; Chirgadzhe, N. Y.; Pauls, H. W. Discovery of inhibitors of the mitotic kinase TTK based on N-(3-(3-sulfamoylphenyl)-1H-indazol-5-yl)-acetamides and carboxamides. *Bioorg. Med. Chem.* **2014**, *22*, 4968–4997. (c) Tardif, K. D.; Rogers, A.; Cassiano, J.; Roth, B. L.; Cimbora, D. M.; McKinnon, R.; Peterson, A.; Douce, T. B.; Robinson, R.; Dorweiler, I.; Davis, T.; Hess, M. A.; Ostanin, K.; Papac, D. I.; Baichwal, V.; McAlexander, I.; Willardsen, J. A.; Saunders, M.; Christophe, H.; Kumar, D. V.; Wettstein, D. A.; Carlson, R. O.; Williams, B. L. Characterization of the Cellular and Antitumor Effects of MPI-0479605, a Small-

Molecule Inhibitor of the Mitotic Kinase Mps1. *Mol. Cancer Ther.* **2011**, *10*, 2267–2275.

(9) (a) Martinez, R.; Blasina, A.; Hallin, J. F.; Hu, W.; Rymer, I.; Fan, J.; Hoffman, R. L.; Murphy, S.; Marx, M.; Yanochko, G.; Trajkovic, D.; Dinh, D.; Timofeevski, S.; Zhu, Z.; Sun, P.; Lappin, P. B.; Murray, B. W. Mitotic Checkpoint Kinase Mps1 Has a Role in Normal Physiology which Impacts Clinical Utility. *PLoS One* **2015**, *10*, e0138616.

(b) Wengner, A. M.; Siemeister, G. Combination of a imidazopyridazine derivative and a mitotic agent for the treatment of cancer. Patent WO2014198776A1, December 18, 2014. (c) Wengner, A. M.; Siemeister, G. Combinations for the treatment of cancer comprising a mps-1 kinase inhibitor and a mitotic inhibitor. Patent WO2014198645, December 18, 2014. (d) Maia, A. R. R.; de Man, J.; Boon, U.; Janssen, A.; Song, J.-Y.; Omerzu, M.; Sterrenburg, J. G.; Prinsen, M. B. W.; Willemsen-Seegers, N.; de Roos, J. A. D. M.; van Doornmalen, A. M.; Uitdehaag, J. C. M.; Kops, G. J. P. L.; Jonkers, J.; Buijsman, R. C.; Zaman, G. J. R.; Medema, R. H. Inhibition of the spindle assembly checkpoint kinase TTK enhances the efficacy of docetaxel in a triple-negative breast cancer model. *Ann. Oncol.* **2015**, *26*, 2180.

(10) (a) Kusakabe, K.-i.; Ide, N.; Daigo, Y.; Tachibana, Y.; Itoh, T.; Yamamoto, T.; Hashizume, H.; Hato, Y.; Higashino, K.; Okano, Y.; Sato, Y.; Inoue, M.; Iguchi, M.; Kanazawa, T.; Ishioka, Y.; Dohi, K.; Kido, Y.; Sakamoto, S.; Yasuo, K.; Maeda, M.; Higaki, M.; Ueda, K.; Yoshizawa, H.; Baba, Y.; Shiota, T.; Murai, H.; Nakamura, Y. Indazole-Based Potent and Cell-Active Mps1 Kinase Inhibitors: Rational Design from Pan-Kinase Inhibitor Anthrapyrazolone (SP600125). *J. Med. Chem.* **2013**, *56*, 4343–4356. (b) Hewitt, L.; Tighe, A.; Santaguidea, S.; White, A. M.; Jones, C. D.; Musacchio, A.; Green, S.; Taylor, S. S. Sustained Mps1 activity is required in mitosis to recruit O-Mad2 to the Mad1-C-Mad2 core complex. *J. Cell Biol.* **2010**, *190*, 25–34. (c) Langdon, S. R.; Westwood, I. M.; van Montfort, R. L. M.; Brown, N.; Blagg, J. Scaffold-Focused Virtual Screening: Prospective Application to the Discovery of TTK Inhibitors. *J. Chem. Inf. Model.* **2013**, *53*, 1100–1112. (d) Chu, M. L. H.; Chavas, L. M. G.; Douglas, K. T.; Eyers, P. A.; Taberner, L. Crystal Structure of the Catalytic Domain of the Mitotic Checkpoint Kinase Mps1 in Complex with SP600125. *J. Biol. Chem.* **2008**, *283*, 21495–21500. (e) Kwiatkowski, N.; Jelluma, N.; Filippakopoulos, P.; Soundararajan, M.; Manak, M. S.; Kwon, M.; Choi, H. G.; Sim, T.; Deveraux, Q. L.; Rottmann, S.; Pellman, D.; Shah, J. V.; Kops, G. J. P. L.; Knapp, S.; Gray, N. S. Small-molecule kinase inhibitors provide insight into Mps1 cell cycle function. *Nat. Chem. Biol.* **2010**, *6*, 359–368. (f) Santaguidea, S.; Tighe, A.; D'Alise, A. M.; Taylor, S. S.; Musacchio, A. Dissecting the role of MPS1 in chromosome biorientation and the spindle checkpoint through the small molecule inhibitor reversine. *J. Cell Biol.* **2010**, *190*, 73–87. (g) Kusakabe, K.-i.; Ide, N.; Daigo, Y.; Itoh, T.; Yamamoto, T.; Kojima, E.; Mitsuoka, Y.; Tadano, G.; Tagashira, S.; Higashino, K.; Okano, Y.; Sato, Y.; Inoue, M.; Iguchi, M.; Kanazawa, T.; Ishioka, Y.; Dohi, K.; Kido, Y.; Sakamoto, S.; Ando, S.; Maeda, M.; Higaki, M.; Yoshizawa, H.; Murai, H.; Nakamura, Y. A unique hinge binder of extremely selective aminopyridine-based Mps1 (TTK) kinase inhibitors with cellular activity. *Bioorg. Med. Chem.* **2015**, *23*, 2247–2260.

(11) (a) Caldarelli, M.; Angiolini, M.; Disingrini, T.; Donati, D.; Guanci, M.; Nuvoloni, S.; Poster, H.; Quartieri, F.; Silvagni, M.; Colombo, R. Synthesis and SAR of new pyrazolo[4,3-*h*]quinazoline-3-carboxamide derivatives as potent and selective MPS1 kinase inhibitors. *Bioorg. Med. Chem. Lett.* **2011**, *21*, 4507–4511. (b) Colombo, R.; Caldarelli, M.; Mennecozzi, M.; Giorgini, M. L.; Sola, F.; Cappella, P.; Perrera, C.; Depaolini, S. R.; Rusconi, L.; Cucchi, U.; Avanzi, N.; Bertrand, J. A.; Bossi, R. T.; Pesenti, E.; Galvani, A.; Isacchi, A.; Colotta, F.; Donati, D.; Moll, J. Targeting the Mitotic Checkpoint for Cancer Therapy with NMS-P715, an Inhibitor of MPS1 Kinase. *Cancer Res.* **2010**, *70*, 10255–10264.

(12) Liu, Y.; Lang, Y.; Patel, N. K.; Ng, G.; Laufer, R.; Li, S.-W.; Edwards, L.; Forrest, B.; Sampson, P. B.; Feher, M.; Ban, F.; Awrey, D. E.; Beletskaya, I.; Mao, G.; Hodgson, R.; Plotnikova, O.; Qiu, W.; Chirgadze, N. Y.; Mason, J. M.; Wei, X.; Lin, D. C.-C.; Che, Y.; Kiarash, R.; Madeira, B.; Fletcher, G. C.; Mak, T. W.; Bray, M. R.; Pauls, H. W. The discovery of orally bioavailable tyrosine threonine kinase (TTK)

inhibitors: 3-(4-(heterocyclyl)phenyl)-1H-indazole-5-carboxamides as anticancer agents. *J. Med. Chem.* **2015**, *58*, 3366–3392.

(13) Kusakabe, K.-i.; Ide, N.; Daigo, Y.; Itoh, T.; Higashino, K.; Okano, Y.; Tadano, G.; Tachibana, Y.; Sato, Y.; Inoue, M.; Wada, T.; Iguchi, M.; Kanazawa, T.; Ishioka, Y.; Dohi, K.; Tagashira, S.; Kido, Y.; Sakamoto, S.; Yasuo, K.; Maeda, M.; Yamamoto, T.; Higaki, M.; Endoh, T.; Ueda, K.; Shiota, T.; Murai, H.; Nakamura, Y. Diaminopyridine-Based Potent and Selective Mps1 Kinase Inhibitors Binding to an Unusual Flipped-Peptide Conformation. *ACS Med. Chem. Lett.* **2012**, *3*, 560–564.

(14) The inherent acid lability of the Boc group prevented further development (further details will be published in due course).

(15) Hopkins, A. L.; Groom, C. R.; Alex, A. Ligand efficiency: a useful metric for lead selection. *Drug Discovery Today* **2004**, *9*, 430–431.

(16) Innocenti, P.; Woodward, H.; O'Fee, L.; Hoelder, S. Expanding the scope of fused pyrimidines as kinase inhibitor scaffolds: synthesis and modification of pyrido[3,4-*d*]pyrimidines. *Org. Biomol. Chem.* **2015**, *13*, 893–904.

(17) Bavetsias, V.; Atrash, B.; Naud, S. G. A.; Shelldrake, P. W.; Blagg, J. Preparation of pyrrolopyridinamine derivatives as Mps1 inhibitors. Patent WO2012123745A1, September 20, 2012.

(18) Dave, C. G.; Shah, P. R.; Desai, V. B.; Srinivasan, S. Pyridopyrimidines. Part I. Synthesis and biological activity of 2-thiopyrido[2,3-*d*]pyrimidin-4(3H)ones. *Indian J. Chem., Sect. B* **1982**, *21B*, 750–752.

(19) Lovering, F.; Bikker, J.; Humblet, C. Escape from Flatland: Increasing Saturation as an Approach to Improving Clinical Success. *J. Med. Chem.* **2009**, *52*, 6752–6756.

(20) Copeland, R. A. *Evaluation of Enzyme Inhibitors in Drug Discovery*; Wiley: Hoboken, NJ, 2005; Vol. 46.

(21) Pesson, M.; Chabassier, S. Nitriles and amide-oximes of 8-alkyl-5-oxo-5,8-dihydro[2,3-*d*]pyrido-6-pyrimidinecarboxylic acids. *C. R. Seances Acad. Sci., Ser. C* **1974**, *279*, 413–415.

(22) (a) Ajiro, K.; Nishimoto, T. Specific site of histone H3 phosphorylation related to the maintenance of premature chromosome condensation. Evidence for catalytically induced interchange of the subunits. *J. Biol. Chem.* **1985**, *260*, 15379–15381. (b) Juan, G.; Traganos, F.; James, W. M.; Ray, J. M.; Roberge, M.; Sauve, D. M.; Anderson, H.; Darzynkiewicz, Z. Histone H3 phosphorylation and expression of cyclins A and B1 measured in individual cells during their progression through G2 and mitosis. *Cytometry* **1998**, *32*, 71–77.

(23) Honold, K.; Paul, J.; Roeschlaub, C.; Schaefer, W.; Scheiblich, S.; Von, H.; Thomas, Whittle, A. Preparation of 7H-pyrido[3,4-*d*]pyrimidin-8-ones as protein kinase inhibitors. Patent WO2007088014A1, August 9, 2007.

(24) Kabsch, W. Software XDS for image rotation, recognition and crystal symmetry assignment. *Acta Crystallogr., Sect. D: Biol. Crystallogr.* **2010**, *66*, 125–132.

(25) Winn, M. D.; Ballard, C. C.; Cowtan, K. D.; Dodson, E. J.; Emsley, P.; Evans, P. R.; Keegan, R. M.; Krissinel, E. B.; Leslie, A. G. W.; McCoy, A.; McNicholas, S. J.; Murshudov, G. N.; Pannu, N. S.; Potterton, E. A.; Powell, H. R.; Read, R. J.; Vagin, A.; Wilson, K. S. Overview of the CCP4 suite and current developments. *Acta Crystallogr., Sect. D: Biol. Crystallogr.* **2011**, *67*, 235–242.

(26) Evans, P. Scaling and assessment of data quality. *Acta Crystallogr., Sect. D: Biol. Crystallogr.* **2006**, *62*, 72–82.

(27) McCoy, A. J.; Grosse-Kunstleve, R. W.; Adams, P. D.; Winn, M. D.; Storoni, L. C.; Read, R. J. Phaser crystallographic software. *J. Appl. Crystallogr.* **2007**, *40*, 658–674.

(28) Emsley, P.; Cowtan, K. Coot: model-building tools for molecular graphics. *Acta Crystallogr., Sect. D: Biol. Crystallogr.* **2004**, *60*, 2126–2132.

(29) Bricogne, G.; Blanc, E.; Brandl, M.; Flensburg, C.; Keller, P.; Paciorek, W.; Roversi, P.; Sharff, A.; Smart, O. S.; Vonrhein, C.; Womack, T. O. *BUSTER*, version 2.11.4; Global Phasing Ltd.: Cambridge, U.K., 2012.

(30) Adams, P. D.; Afonine, P. V.; Bunkóczi, G.; Chen, V. B.; Davis, I. W.; Echols, N.; Headd, J. J.; Hung, L.-W.; Kapral, G. J.; Grosse-Kunstleve, R. W.; McCoy, A. J.; Moriarty, N. W.; Oeffner, R.; Read, R. J.; Richardson, D. C.; Richardson, J. S.; Terwilliger, T. C.; Zwart, P. H.

PHENIX: a comprehensive Python-based system for macromolecular structure solution. *Acta Crystallogr., Sect. D: Biol. Crystallogr.* **2010**, *66*, 213–221.

(31) Smart, O. S.; Womack, T. O.; Sharff, A.; Flensburg, C.; Keller, P.; Paciorek, W.; Vonrhein, C.; Bricogne, G. *Grade*, version 1.2.1; Global Phasing Ltd.: Cambridge, U.K., 2012.

(32) Bruno, I. J.; Cole, J. C.; Lommerse, J. P. M.; Rowland, R. S.; Taylor, R.; Verdonk, M. L. Isostar: a library of information about nonbonded interactions. *J. Comput.-Aided Mol. Des.* **1997**, *11*, 525–537.

(33) Davis, I. W.; Leaver-Fay, A.; Chen, V. B.; Block, J. N.; Kapral, G. J.; Wang, X.; Murray, L. W.; Arendall, W. B.; Snoeyink, J.; Richardson, J. S.; Richardson, D. C. MolProbity: all-atom contacts and structure validation for proteins and nucleic acids. *Nucleic Acids Res.* **2007**, *35*, W375–W383.

(34) Workman, P.; Aboagye, E. O.; Balkwill, F.; Balmain, A.; Bruder, G.; Chaplin, D. J.; Double, J. A.; Everitt, J.; Farningham, D. A. H.; Glennie, M. J.; Kelland, L. R.; Robinson, V.; Stratford, I. J.; Tozer, G. M.; Watson, S.; Wedge, S. R.; Eccles, S. A. Guidelines for the welfare and use of animals in cancer research. *Br. J. Cancer* **2010**, *102*, 1555–1577.